Environmental Science Nano

ROYAL SOCIETY OF CHEMISTRY

CRITICAL REVIEW

View Article Online
View Journal

Cite this: DOI: 10.1039/d2en00600f

Environmental routes of virus transmission and the application of nanomaterial-based sensors for virus detection

Wei Wang, †[ab] Seju Kang, †[ab] Wei Zhou [c] and Peter J. Vikesland *[ab]

Received 21st June 2022,
Accepted 18th November 2022

DOI: 10.1039/d2en00600f

rsc.li/es-nano

Many outbreaks of emerging disease (*e.g.*, avian influenza, SARS, MERS, Ebola, COVID-19) are caused by viruses. In addition to direct person-to-person transfer, the movement of these viruses through environmental matrices (water, air, and food) can further disease transmission. There is a pressing need for rapid and sensitive virus detection in environmental matrices. Nanomaterial-based sensors (nanosensors), which take advantage of the unique optical, electrical, or magnetic properties of nanomaterials, exhibit significant potential for environmental virus detection. Interactions between viruses and nanomaterials (or recognition agents on the nanomaterials) can induce detectable signals and provide rapid response times, high sensitivity, and high specificity. Facile and field-deployable operations can be envisioned due to the small size of the sensing elements. In this frontier review, we summarize virus transmission *via* environmental pathways and then comprehensively discuss recent applications of nanosensors to detect various viruses. This review provides guidelines for virus detection in the environment through the use of nanosensors as a tool to decrease environmental transmission of current and emerging diseases.

Environmental significance

Numerous viruses (including SARS-CoV-2) can spread across various environmental matrices (*e.g.*, air, soil, water, and food), promoting direct/indirect infection transmission. Environmental monitoring of viruses is highly desirable to prevent the spread of infectious diseases. Nanomaterial-based sensors (nanosensors) have recently shown great potential for virus detection with low-cost, high sensitivity, and short analysis time. The small size and the adaptability of nanosensors enable field-deployable virus detection in various environmental matrices. This review provides guidelines for nanosensor application for virus detection to control the environmental transmission of current and emerging diseases associated with viruses.

1. Introduction

Respiratory viruses can spread from person to person and cause contagious respiratory illnesses. Outbreaks of viral disease have regularly occurred and have caused hundreds of thousands of fatalities over the last three decades: severe acute respiratory syndrome coronavirus (SARS-CoV) in 2003,[1] influenza A virus H1N1 subtype in 2009,[2] Ebola virus (EBOV) in 2014,[3] middle east respiratory syndrome coronavirus (MERS-CoV) in 2014,[4] and Zika virus (ZIKV) in 2014.[5] Currently, the ongoing COVID-19 (caused by the SARS-CoV-2 virus) pandemic is the world's most pressing public health threat and as of June 2022 has resulted in known infections in greater than 529 million people across the world.[6] To minimize morbidity and mortality, rapid virus detection and contact tracing along routes of virus transmission are crucial.[7] In addition to direct transfer between infectious and susceptible individuals, viruses can also be transmitted through environmental media such as water, air, and food.[8] For instance, SARS-CoV-2 spreads not only through person-to-person contact, but also *via* contaminated fomites and respiratory aerosols.[9] The survival and transport of viruses within and across environmental matrices promotes indirect transmission.[10] Detection of viruses in these environmental matrices is required to fully track all routes of virus transmission, determine undiagnosed infections at the population/community level,[11] and control the spread of disease.

Current virus detection methods include plaque assay, polymerase chain reaction (PCR) based techniques, loop-mediated isothermal amplification (LAMP), and enzyme-

[a] *Department of Civil and Environmental Engineering, Virginia Tech, Blacksburg, Virginia 24061, USA. E-mail: pvikes@vt.edu*
[b] *Virginia Tech Institute of Critical Technology and Applied Science (ICTAS) Sustainable Nanotechnology Center (VTSuN), Blacksburg, Virginia 24061, USA*
[c] *Department of Electrical and Computer Engineering, Virginia Tech, Blacksburg, Virginia 24061, USA*
† These authors contribute equally to the work.

linked immunosorbent assay (ELISA). The standardized operation procedures and high sensitivity of these methods render them widely applicable, but primarily located in clinical or laboratory settings. Tedious pretreatment steps and huge investments in chemicals or instruments often hamper their application for environmental samples, especially for the large number of samples required to track viral transmission routes. There is an urgent need for lower-cost, field deployable devices, as well as high sensitivity and specificity that consider environmental diagnostic applications.

Nanomaterial-based sensors (nanosensors) have shown significant promise towards virus detection in the environment due to their small size, low-cost, high sensitivity, and rapid turnaround time. Fig. 1 summarizes the principal components of a nanosensor. The basic principle is to transform stimuli arising from the interaction between a given nanomaterial and a target analyte of interest into a quantifiable signal, termed signal transduction. Nanosensors employ a range of signal transduction mechanisms enabled by functionalizing nanomaterials with different recognition elements such as aptamers, peptides, and antibodies,[12] that render high specificity. Three types of signal transduction have been broadly applied in nanosensors: optical, electrical, and magnetic.[13] Such signal transduction enables higher sensitivity and stability over traditional methods. Nanomaterials have several advantages over bulk materials. Nanomaterials have completely different physiochemical properties (*e.g.*, durability, conductivity, and quantum effects at nanoscale) from those of bulk materials. Also, they have high surface-to-volume ratio which help close contact with surrounding macromolecules (*e.g.*, DNA, virus, protein), thus affecting reactivity. Different nanoparticle morphologies and properties can be harnessed for nanosensor development. Plasmonic nanomaterials such as gold and silver nanoparticles (AuNPs, AgNPs) or photoconductive materials (*e.g.*, carbon nanotubes (CNTs)) have been used to develop optical nanosensors. For the development of electrical nanosensors, both one-dimensional nanomaterials (*e.g.*, silicon nanowires (SiNWs), CNTs) and two-dimensional nanomaterials (*e.g.*, graphene/graphene oxide (GO) and metal–organic frameworks (MOFs) nanosheets) have been used. Lastly, iron-based nanoparticles (*e.g.*, Fe^0, Fe_3O_4, γ-Fe_2O_3) are commonly used to develop magnetic nanosensors. Such nanomaterials can be incorporated within flexible substrates such as paper or lateral flow-devices to be low-cost and field-deployable and are thus suitable for environmental applications. Despite these advantages, the application of nanosensors for virus detection in the environment still has not been heavily explored. In this review, we emphasize the necessity of virus detection in environmental matrices by introducing environmental viral transmission routes and then review the latest progress toward the developments of nanosensors for virus detection to discuss the feasibility and potential challenges for their application for environmental sample interrogation.

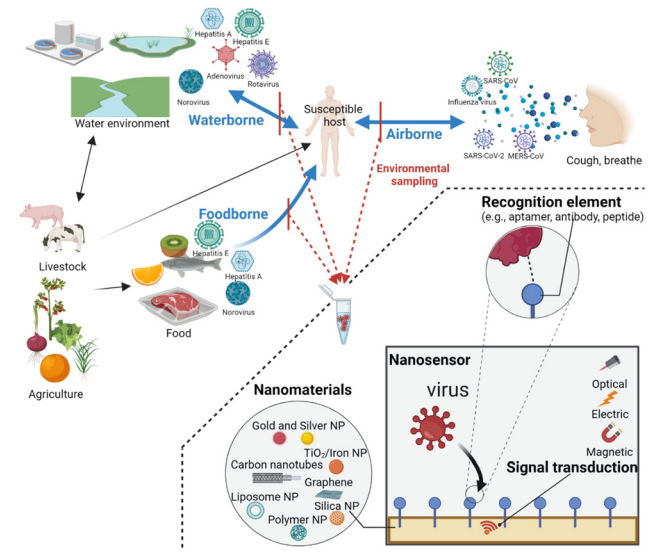

Fig. 1 Schematic diagram of three major virus transmission pathways (*i.e.*, waterborne, airborne, and foodborne) to a susceptible host and the application of nanosensors for virus detection. Environmental sampling is followed by nanosensor-enabled detection of viruses. The principal components of a nanosensor for virus detection include signal transduction, recognition element, and nanomaterials.

2. Virus transmission routes in the environment

Viruses can spread in the environment and infect people through inhalation and ingestion. Water, air, and food are key environmental media known to play a role in virus transmission (Fig. 1).[14] For example, viruses can be discharged into sewage along with the feces of infected people or animals and can spread when water circulates or when transmitted into the air.[15] Droplets and aerosol particles produced when infected patients cough, sneeze, speak, and breathe are important carriers for the environmental distribution of viruses.[16] Viruses may also spread disease through the food chain or contact between infected individuals and prepared foods. Detection of viruses in these different environments is required to track the routes of virus transmission.

2.1 Waterborne transmission

Waterborne viruses such as hepatitis A and E virus (HAV and HEV), norovirus (NoV), adenovirus (AdV), and rotavirus (RV) are enterally transmitted and are primary causes of waterborne disease.[17] One obvious route of waterborne virus transmission is the discharge of sewage and sewage-contaminated waters into drinking water sources. Wastewater is considered one of the most concentrated environmental virus reservoirs with an estimated mean concentration of 7000 infectious enteric viruses per liter since viruses are discharged into sewage along with the feces and urine of

infected people or animals.[18] High titers of the infectious virus have been measured in wastewater samples collected worldwide.[19,20] For example, SARS-CoV-2 RNA has been detected in wastewater and can be used as a potential early warning system for COVID-19 transmission in the community.[21–23] Although some wastewater treatment processes may remove viruses, their removal efficiency is often limited. One report suggests that primary treatment achieves only ~1 $\log_{10}$ removal of NoV.[24] The same study found that activated sludge was more effective for NoV removal (2.3–3.1 $\log_{10}$) than trickling filters, biological aerated filters, and humus tanks. Further, UV disinfection of the final effluent only led to 0.8–1 $\log_{10}$ NoV reduction. Hence, viable viruses can be released into environmental waters *via* the discharge of treated effluent. Pang *et al.* investigated the occurrence of viruses in six major rivers in Alberta by quantitative PCR (qPCR) after concentrating samples by the adsorption–elution method and found that RV was the most prevalent virus (concentrations ranging from 2.3 to 4.5 $\log_{10}$ genomic equivalent copies per liter) and had a seasonal peak during winter.[25] NoV, sapovirus, astrovirus, AdV, and John Cunningham virus also peaked during the winter. Some viruses are environmentally resilient and may be transmitted through surface water, groundwater, and drinking water resources. Lee *et al.* investigated the occurrence of NoV in 71 sampling sites in South Korea by reverse transcription (RT)-PCR after concentrating samples by the adsorption–elution technique, and found that 48.3% (summer) and 35.3% (fall–winter) of the samples were positive.[26] Miura *et al.* collected river water samples at 21 drinking water treatment plants in Japan from June 2017 to August 2018 by RT-PCR after concentrating sample by adsorption–elution technique and found that the detection rate for NoV GII (gene type) and RV (group A) were 87% and 100%, respectively.[27] Fortunately, the total number of viral reads at the point of use (*e.g.*, tap water) was ~0.1% of that in raw river water except for HEV where it was 2.2%.[28] Although the risk of getting infected by viruses in tap water is expected to be relatively low due to their concentrations, there remains a possibility of transmission to other environments during outbreaks. In addition, evidence indicates the presence of viable viruses in aquatic matrices such as seawater and reuse water.[29,30]

2.2 Airborne transmission

Airborne viruses are transmitted by aerosolized droplets or particles produced when infected individuals cough, sneeze, speak, and breathe.[16,31] Droplets and aerosol particles produced by these respiratory activities span a wide range of sizes, and some can remain suspended in the air for seconds to hours, can travel long distances, and can accumulate in poorly ventilated spaces.[32] Aerosol-based dissemination can lead to the widespread transmission of viruses. Influenza, measles, and coronavirus (SARS-CoV or SARS-CoV-2) are well-known airborne viruses.[16,33–35]

Airborne virus concentrations are highest in indoor environments characterized by poor ventilation, large numbers of people, confined space, and the presence of viral sources. For example, a hospital is one environment where viruses can quite readily spread through the air from infected individuals. Researchers have found that influenza viral RNA could be detected in fever clinics for confirmed flu patients and visitors although there were no viruses in the outpatient hall and clinical laboratory.[36] Similarly, SARS-CoV-2 RNA was detected with a concentration of several gene copies per cubic meters in aerosols from patient toilet areas in Fangcang Field Hospital in Wuhan by collecting aerosol samples on a filter, extracting RNA in dissolved solution and analyzing by PCR.[37] The concentrations of airborne viruses in most places within hospitals (isolation wards and ventilated patient rooms) are usually low thus suggesting that room ventilation and open spaces can effectively reduce viral loads. Schools and offices are crowded public places at high-risk of airborne virus transmission, especially during the flu season. Xie *et al.* investigated the occurrence of several airborne viruses in air samples collected by bioaerosol samplers in a university campus by RT-PCR and found that influenza A and B viruses were detectable at higher frequencies than other viruses (rhinovirus, respiratory syncytial virus, and human coronavirus).[38] The school corridor had the highest influenza A virus concentration relative to classrooms and gyms in an elementary school due to the high passing frequency and air turbulence caused by students' activities.[39] In contrast, the influenza A virus was not detected in any tested outdoor samples. Besides the physical spaces, the indoor environment conditions such as temperature and relative humidity (RH) have been identified as important factors in airborne virus survival and transmission.[40,41] Cold temperatures and low RH favor the spreading of airborne viruses due to their positive effects on virus stability.[42]

2.3 Foodborne transmission

Foodborne viruses are a significant cause of human morbidity and mortality. Fresh food can be contaminated at any step between preharvest and postharvest.[43] Foodborne viral infections are often transmitted *via* the fecal–oral route through ingesting contaminated food and illness across the food chain.[44] HAV and NoV are recognized as two of the most important foodborne viruses[43,45] and are regularly detected in shellfish, fresh fruits, and vegetables. SARS-CoV-2 is also detected from frozen cod packaging.[46]

Using contaminated irrigation water and agricultural soils is a primary route of viral transmission during preharvest. The transfer of viruses from irrigation water to plants can occur through direct contact or internalization into plant tissue *via* the root system.[44] In field experiments, Brassard *et al.* found that although the concentration of viruses in irrigation water was extremely low, NoV and swine HEV could be detected in strawberry samples after being irrigated with contaminated water for several days.[47] These results indicate

that fruits might concentrate the viruses during the growth to pose a threat to human beings. Similar results were found in some fresh fruits and vegetables and their associated agricultural and environmental samples in South Korea.[48] These results suggest that removing viruses from irrigation water may successfully minimize the transmission of foodborne viruses during preharvest.

During harvest and postharvest, foodborne viruses can be traced to foods handled by infected food handlers (*e.g.*, field harvesters, production plant workers, professional chefs). Shellfish, fruits, and vegetables are at high risk for transmitting viruses since they undergo extensive human handling during production. To check whether the infected food handlers will cause secondary contamination in food samples, Somura *et al.* recovered NoV in food samples using bacterial culture method in Tokyo from five NoV outbreaks during 2015–2016. It was found that each partial NoV *VP1* sequence of NoV-positive food samples matched completely with those in NoV-positive individuals and food handlers, which proved food handlers played a potentially important role in NoV transmission.[49] Similar results have been obtained by other researchers that food handling practices carry potential risk of acute gastroenteritis outbreaks.[50] Besides, recent research has shown that SARS-CoV-2 can remain highly stable on frozen food and that contaminated cold-storage foods may pose a risk for SARS-CoV-2 transmission between countries and regions.[51] These results indicate that the development of safe food-handling strategies among food handlers is important in controlling the transmission of foodborne viruses.

2.4 Current virus detection approaches

Before discussing nanosensor applications for virus detection, we briefly summarize current approaches to virus detection. The standard method to detect the pathogenic virus is the plaque assay. The plaque assay counts the number of plaque-forming units (PFU) in a certain volume of liquid. In this assay, various virus dilutions are incubated in the presence of a monolayer of recipient host cells. A viral plaque forms when the virus infects the recipient cells. The viral concentration is then determined using either PFU or the 50% tissue culture infectious dose ($TCID_{50}$). The plaque assay has several limitations, such as the required long incubation period for plaque formation, laborious counting effort, and the limited availability of recipient host cells for many viruses of health concern.[52]

Nucleic acid amplification strategies such as PCR and LAMP have been widely used to detect viruses.[53,54] PCR and LAMP approaches require the extraction of DNA or RNA from a virus. Following this step, enzyme-linked gene amplification enables the detection of target genes. For RNA detection, extracted RNA needs to be reverse-transcribed to complementary DNA using a reverse transcriptase enzyme prior to amplification. PCR generally relies upon *Taq* polymerase to replicate the target gene over multiple thermal cycles. For this process, two primers are designed to target the amplified gene region. In contrast, LAMP relies upon four different primers that bind to six distinct regions of target DNA. *Bst* polymerase is used to displace strands at a constant temperature and replicate the target gene. LAMP has greater specificity and a shorter turnaround time (~0.5 to 1 hour) than PCR. Further, PCR approaches require skilled personnel and high-cost facilities.[55] Such an entry barrier limits the proactive detection of infectious viruses. While LAMP is gaining attention as a PCR alternative owing to its fast turnaround time and field deployability, the high rate of false positives makes the development of LAMP-based assays challenging.[56–58] RT-PCR and RT-LAMP assays for detection of SARS-CoV-2 have LODs of 484 and 200 copies per mL.[59,60]

ELISA can detect viruses using selective complexation between an antigen and an antibody linked to an enzyme. A specific antibody conjugated substrate is used to capture the target virus, followed by an enzyme attachment. Commonly, horseradish peroxidase (HRP)-conjugated goat anti-mouse immunoglobulin (IgG) is used as the enzyme. HRP catalyzes the oxidation of 3′,5,5′-tetramethylbenzidine (TMB) by hydrogen peroxide (H_2O_2) and the optical signal arising from the production of oxidized TMB enables virus detection. ELISA assay for detection of SARS-CoV-2 IgG has a LOD of 0.0736 μg mL^{-1}.[61] Despite its success in virus detection, ELISA suffers from laborious assay procedures and poor sensitivity under real-world application conditions.[62]

3. Applications of nanosensors for virus detection

Due to the unique optical, electrical, or magnetic properties, nanosensors have shown significant potential for virus detection. This section comprehensively discusses recent nanosensor applications for virus detection. We summarize the discussed nanosensors in Table 1 for SARS-CoV-2, Table 2 for influenza virus due to their focus in recent times and the massive reference databases, and Table 3 for other viral targets. In each table, we conclude the main recognition elements, sensing strategy and the limit of detection (LOD) of each sensor. LOD is one of the most important criteria to be considered for environmental application, especially for tracking virus transmission in which viral concentration may go down to zero if the distance away from a source is far. We emphasize that the LODs and units listed in the tables reflect those reported in the original work. While conversion of these units into a standardized set of reporting units would be ideal, it was considered outside the scope of the present work due to the many assumptions required for such calculations.

3.1 Optical nanosensors

Nobel metal (*e.g.*, Au or Ag) NPs can support localized surface plasmon resonance (LSPR) modes,[63,64] the collective oscillation of conductive band electrons in metal NPs by free-

Table 1 Summary of nanosensors for the detection of SARS-CoV-2

Method	Recognition element	General approach	LOD	Ref.
Optical				
Colorimetric	Antibody	Colloidal AuNPs functionalized with antibodies targeted viral proteins and the extinction spectrum showed red-shifted	Equivalent to the C_t of 36.5 for PCR	78
SERS	ACE2	Au nanoneedles functionalized with ACE2 targeted viral S protein, exhibiting SERS signals of SARS-CoV-2	80 copies per mL	103
SERS	ACE2	Ag nanorod array functionalized with ACE2 targeted viral S protein, quenching, and shifting the SERS signals of ACE2	N/A	104
SERS	Aptamer	Au nanopopcorn array functionalized with aptamer targeted viral S protein, releasing the aptamer with the Raman reporter	$<$10 PFU mL^{-1}	111
Fluorometric	ACE2	SWCNTs functionalized with ACE2 targeted viral S protein, leading to fluorescence increases	12.6 nM	122
Electrical				
Electrochemical	EDC/NHS	GO-based electrodes functionalized with AuNS and EDC/NHS interacted with viral glycoprotein, leading to a differentiable DPV	1.68×10^{-22} μg mL^{-1}	151
Electrochemical	Aptamer	AuNPs functionalized with ssDNA targeted viral RNA and immobilized on an electrochemical platform, leading to output voltage changes	6.9 copies per μL	161
Electrochemical	Aptamer	Au@Fe_3O_4 functionalized with aptamer targeted viral RNA and captured on rGO-based platform, resulting in high conductivity	200 copies per mL	162
Electrochemical	Aptamer	SiNPs functionalized with redox dyes and aptamer targeted viral N gene and captured by aptamer functionalized magnetic NPs, resulting in DPV changes	1 copy per μL	163
FET	Antibody	Graphene-based FET functionalized with antibody targeted virus and viral spike protein, inducing electrical signal changes	16 PFU mL^{-1}, 242 copies per mL	179
FET	Antibody	WSe_2 based FET functionalized with antibody through 11-MUA targeted virus and viral spike protein, inducing electrical signal changes	25 fg μL^{-1}	180
FET	ACE2	A dual-gate FET functionalized ACE2 captured virus and the voltage shift was analyzed at the reference current	165 copies per mL	185
FET	Aptamer	PLL is functionalized on surface of graphene-FET to immobilize DNA probes. The electrical signals were measured when applying for viral RNA detection	1 fM	187

space light excitation, to concentrate intense optical fields at the nanoscale.[65] Therefore, such plasmonic nanomaterials have been used as highly sensitive optical nanosensors across the fields of analytics, food safety, biomedicine, and environmental science.[66–70] Fluorescent nanomaterials, such as semiconductor quantum dots (QDs)[71,72] and lanthanide-doped NPs,[73] can serve as down-conversion and up-conversion fluorescence emission nanoprobes for fluorometric sensing approaches.

To date, several virus sensing approaches have been developed that rely upon optical nanomaterials. Because of the large volume of literature on optical nanosensors, herein we exclude works on the detection of viral nucleic acid that precedes gene amplification (*e.g.*, plasmonic NP-based-colorimetric method coupled with PCR for detection of SARS-CoV-2 RNA[74]). More detailed reviews on viral nucleic acid detection using optical nanosensors can be found in the recent literature.[75,76] The following section splits into three parts according to the optical signal readout device: colorimetric, surface-enhanced Raman scattering (SERS), and fluorometric.

3.1.1 Colorimetric nanosensors. Colloidal noble metal NPs can be uniformly dispersed in suspension. The color of noble metal NPs reflects the LSPR resonant absorption and scattering properties depending on their sizes, shapes, and the surrounding local environment.[77] Notably, Au and Ag NPs of the same shape and size can exhibit different colors in the visible to near-infrared (NIR) region due to the additional interband-transition induced optical absorption in AuNPs. Colorimetric sensing approaches generally rely upon color changes that can be measured by a UV-vis spectrophotometer or identified by the naked eye. Aggregation of noble metal NPs through conjugation with a target virus results in an absorbance peak shift (*i.e.*, red-shift). Recently, AuNPs functionalized with antibodies targeting three SARS-CoV-2 proteins (spike, envelope, membrane) were achieved by colorimetric detection.[78] The absorbance peak (560 nm) of a colloidal suspension of AuNPs exhibited a red-shift a few minutes after mixed with a SARS-CoV-2-containing sample. Often, colloidal plasmonic NPs exhibit non-specific binding in resource-constrained settings due to the high susceptibility of the approach to perturbations in their external environment.[79] To overcome this challenge, Xiong *et al.* induced the disassembly of gold nano-aggregates through contact with enterovirus 71 (EV71).[80] Specifically, negatively charged AuNPs dispersed in solution were aggregated due to the addition of positively charged peptides, resulting in a blue-colored suspension. In the presence of EV71, the target antibody immunoassay system releases a liposome encapsulating multiple enzymes that hydrolyze the positively charged peptide, thus promoting the disassembly of AuNP aggregates. This approach successfully allows EV71 detection with a LOD of 16 copies per μL.

Table 2 Summary of nanosensors for the detection of influenza virus

Method	Virus type	Recognition element	General approach	LOD	Ref.
Optical					
Colorimetric	H1N1, H3N2	Antibody	Au and Fe_3O_4 NPs functionalized with antibody captured the virus and separated by a magnet. AuNPs catalyzed TMB oxidation and turned the aqueous solution color to blue in positive samples	4.42×10^{-14} g mL^{-1} (H1N1), 2.5 PFU mL^{-1} (H3N2)	83
Colorimetric	H3N2	Antibody	Au–CNTs functionalized with antibody captured the virus. Au–CNTs catalyzed TMB oxidation and turned the aqueous solution color to blue in positive samples	3.4 PFU mL^{-1}	84
Colorimetric	H1N1	Peptide	PDA NPs functionalized with peptide captured the virus and it perturbated the backbone of PDA, resulting in the aqueous solution color change from blue to red	10^5 PFU	87
SERS	H1N1	N/A	A high-density tip-to-tip Au concave-shape nanostructured substrate captured the virus	10^4 PFU mL^{-1}	102
SERS	H1N1	Antibody	Au NPs functionalized with antibody and the Raman reporter formed the sandwich structure with the capture substrate in the presence of virus	4.1×10^3 $TCID_{50}$ mL^{-1}	106
SERS	H1N1	Antibody	Au NPs functionalized with antibody and the Raman reporter formed the sandwich structure with the capture substrate in the presence of virus	6 $TCID_{50}$ mL^{-1}	107
SERS	H1N1	OHT	Au NPs functionalized with OHT formed the sandwich with the capture substrate in the presence of oseltamivir-resistant virus	1 PFU	110
SERS	H3N2	Aptamer	Aptamer with the Raman reporter formed the sandwich with the AgNP coated capture substrate in the presence of virus	10^{-4} HAU	113
SERS	H7N9	Antibody	Au@Ag NPs functionalized with the antibody and the Raman reporter was captured on the TL of the LFIA trip in the presence of virus	0.0018 HAU	115
SERS	H1N1	Antibody	Ag@Fe_3O_4 NPs functionalized with the antibody and the Raman reporter enriched the virus from impurities by a magnet and was captured on the TL of the LFIA trip	50 PFU mL^{-1}	117
Fluorometric	H1N1	Antibody	AuNPs and QDs functionalized with the antibody captured the virus and exhibited LSPR-induced fluorescence enhancement in positive samples	0.03 pg mL^{-1} (water); 0.4 pg mL^{-1} (human serum)	125
Fluorometric	H1N1, H3N2	Antibody	AuNP decorated CNTs and QDs functionalized with the antibody captured the virus and exhibited LSPR-induced fluorescence enhancement in positive samples	0.1 pg mL^{-1} (water); 50 PFU mL^{-1} (clinical sample)	126
Fluorometric	H1N1	Antibody	AuNPs and QDs were connected through the peptide chain that was functionalized with antibody. Virus attachment to the peptide chain led to the fluorescence quenching in positive samples	17.02 fg mL^{-1}	128
Fluorometric	H1N1	Antibody	Fluorescent NPs conjugated with the virus were captured on the TL in FICT. The TL/CL ratio was used for quantification	$<$20 HAU mL^{-1}	131
Fluorometric	H7N1, H7N7	Antibody	Fluorescent NPs conjugated with the virus were captured on the TL in FICT. The TL/CL ratio was used for quantification	40 HAU mL^{-1}	133
Fluorometric	H5N1	Aptamer	The aptamer captured the virus and QD fluorescence reporter was released from the quencher	0.4 HAU	134
Electrical					
Electrochemical	H1N1	N/A	AgNPs were adsorbed on a carbon electrode in the presence of H1N1 and current spikes were quantified	Sub pM level	146
Electrochemical	H1N1, H5N1, H7N9	Antibody	ZnONR functionalized with antibody targeted virus. HRP-conjugated detection antibody was captured by virus and oxidized TMB in sensing region, resulting in current changes	1 pg mL^{-1}	150
Electrochemical	H9N2	Antibody	RuSi NPs and magnetic NPs functionalized with antibody captured virus on an Au modified ITO electrode, enhancing ECL signals	14 fg mL^{-1}	157
Chemiresistor	H5N1	Aptamer	CNTs functionalized with DNA probe sequence captured viral DNA, leading to the resistance changes	2 pM	171
FET	H3N2	Antibody	SiNWs functionalized with antibody captured virus, resulting in discrete nanowire conductance changes	10^4 viruses per L	182
FET	H1N1	CMP-NANA	SiNWs functionalized with CMP-NANA through the aldehyde self-aligned monolayer bound to hemagglutinin 1,	1 pM	184

Table 2 *(continued)*

Method	Virus type	Recognition element	General approach	LOD	Ref.
			causing voltage shifts		
FET	H1N1	Aptamer	CNT-FET immobilized with probe DNA hybridized with target DNA. The charge transfer between DNA and CNT led to a decrease of the drain current	1 pM	186
Magnetic					
MR	H1N1	Antibody	Streptavidin-coated magnetic NPs with antibody captured on sensors in the presence of virus, resulting in a resistance change	150 $TCID_{50}$ mL^{-1}	194
MR	H3N2	Antibody	Streptavidin-coated magnetic NPs with antibody captured on a portable GMR platform the presence of virus. The magnetoresistance ratio was measured	125 $TCID_{50}$ mL^{-1}	195
MR	H1N1, H3N2	Antibody	The target virus-detection antibody–magnetic NPs complex was captured by antibody, gave rise to the positive signals	250 $TCID_{50}$ mL^{-1}	196
MRS	N/A	Antibody	Magnetic NPs functionalized with anti-tag captured target, resulting in changes in the spin–spin relaxation time	N/A	198

In place of using an aggregation strategy, AuNPs can also be coupled with an Ag staining technique for colorimetric virus detection. In this approach, silver ions in proximity to an AuNP surface are reduced by a reducing agent. The AuNPs transfer an electron from the reducing agent to a silver ion and catalyze formation of a silver metal film on the AuNP surface. The continuous deposition of silver layer over Au by this process produces a gray color and the intensity of developed color can be monitored. Recently, this technique was applied within a microfluidic device for multiplex virus detection.[81] In this study, the authors used the systematic evolution of ligands by exponential enrichment (SELEX) to generate aptamer recognition elements that have an affinity for ZIKV and chikungunya virus (CHIKV) envelope proteins. In the presence of those proteins, the aptamer functionalized microfluidic device forms a sandwich structure with AuNPs conjugated with the same aptamer. Following sandwich formation, silver reagents were introduced onto the surface of AuNPs, and the silver layer was formed. The intensity of the digitized gray color as measured by ImageJ (CMYK model) showed a linear correlation with the concentration of virus proteins and LODs of 1 pM in phosphate-buffered saline (PBS) and 100 pM in calf blood.

The coupling of plasmonic and magnetic NPs has also been applied in colorimetric assays. It was reported that an aptamer conjugated maghemite (γ-Fe_2O_3) and AuNP hybrid nanocomposite enabled rapid visual detection of dengue virus (DENV).[82] For sensitive detection of influenza A virus H1N1, a magnetic nanozyme-linked immunosorbent assay (MagLISA) was developed (Fig. 2).[83] The enzyme-like activity of AuNPs known as Au nanozymes (AuNZs) catalyzed oxidation of TMB (colorless) by H_2O_2. When TMB is oxidized it produces a blue color. Antibody conjugated Fe_3O_4 and AuNPs form a sandwich complex in the presence of H1N1. This complex can be separated *via* applying a magnetic field and then re-suspended in colorizing agent-containing solution (H_2O_2 and TMB). The color change is then monitored at 450 nm, showing positive linearity with the H1N1 concentration and a LOD of 4.42×10^{-14} g mL^{-1}. Clinically isolated influenza A virus H3N2 from patients could be successfully separated from human serum by this platform and detected with a LOD of 2.5 PFU mL^{-1}. Additionally, other peroxidase-like AuNP-based substrates have been applied for colorimetric virus detection. To improve their catalytic activity, AuNPs can be coupled with CNTs and graphene. For instance, an antibody-conjugated AuNP–CNT hybrid substrate was applied for influenza A virus H3N2 detection.[84] H3N2 was attached to the bottom of a polystyrene 96-well followed by the addition of antibody-conjugated AuNP–CNTs. After several wash cycles to remove non-deposited AuNP–CNTs, a mixture of TMB and H_2O_2 was added. More AuNP–CNTs were attracted in higher concentration virus solutions, which showed higher catalytic activity. In this case, more TMB could be oxidized, resulting in the development of a detectable blue color. This method showed a LOD of 3.4 PFU mL^{-1}. The same procedure was conducted using an AuNP–graphene hybrid substrate to detect NoV-like NPs (NoV-LPs).[85] The LOD of the method was 92.7 pg mL^{-1}.

In place of AuNP-based substrates, vanadium oxide (V_2O_5) NPs have also been applied for peroxidase-like catalytic activity-based colorimetric virus sensing.[86] V_2O_5 NPs have the great catalytic ability and robust stability. V_2O_5-Encapsulated liposomes (VONP-LPs) and Fe_3O_4 NPs were conjugated with an antibody specific to NoV-LPs. After complexation of VONP-LPs, Fe_3O_4 NPs, and NoV-LPs *via* antigen–antibody interactions, the magnetically separated sample was subjected to Triton X induced liposome hydrolysis. The release of V_2O_5 NPs catalyzes the oxidation of TMB by H_2O_2 and produces an intense blue color. The V_2O_5 NPs also enhance the redox signal in the differential pulse voltammetry (DPV) spectrum, thus enabling electrochemical sensing. Linear trends between the concentrations of NoV-LPs and the corresponding optical and electrochemical signals in different ranges were confirmed. The

Table 3 Summary of nanosensors for the detection of other viruses

Method	Virus type	Recognition element	General approach	LOD	Ref.
Optical					
Colorimetric	EV71	Antibody	Liposome functionalized with antibody was retrieved in the presence of the virus. The liposome lysis released multiple enzymes that disassembled AuNP aggregates, resulting in a color change from blue to red	16 copies per μL	80
Colorimetric	ZIKV, CHIKV	Aptamer	AuNPs functionalized with aptamer formed sandwich with the capture substrate in the presence of the virus. Ag reagent addition on the AuNP surface caused color change	1 pM (PBS); 100 pM (calf blood)	81
Colorimetric	DENV	Aptamer	Au and γ-Fe_2O_3 NPs functionalized with aptamer targeted the virus, leading to color change	N/A	82
Colorimetric	NoV-LPs	Antibody	Graphene–AuNPs functionalized with antibody captured the virus. AuNPs catalyzed TMB oxidation and turned the aqueous solution color to blue in positive samples	92.7 pg mL^{-1}	85
Colorimetric	NoV-LPs	Antibody	Fe_2O_3 and V_2O_5 NPs functionalized with antibody captured the virus. AuNPs catalyzed TMB oxidation and turned the aqueous solution color to blue in positive samples	0.34 pg mL^{-1}	86
Colorimetric	RV	Antibody	Au nanopillars functionalized with antibody captured the virus, leading to LSPR peak shift	126 PFU mL^{-1}	89
SERS	PCV2, PPV, PRV	N/A	Porous carbon film coated AgNPs captured the virus	10^7 copies per mL	98
SERS	PVX	Antibody	AuNRs functionalized with aptamer and the Raman reporter formed the sandwich with the Au shell magnetic NPs in the presence of the virus	2.2 ng mL^{-1}	99
SERS	Ad5, Cv3	N/A	Hollow Au nanocones with the opening size for virus loading captured the virus in the vicinity of the SERS hot-spots	N/A	100
SERS	MYXV, CDV, TMV, PVX	N/A	The pore-like Au nano-cavities captured the virus in the vicinity of the SERS hot-spots	N/A	101
SERS	AdV, EMCV	N/A	A high-density tip-to-tip Au concave-shape nanostructured substrate captured the virus in the vicinity of the SERS hot-spots	10^6 PFU mL^{-1}	102
SERS	PRV	Antibody	AuAg@Ag NPs functionalized with the antibody and the Raman reporter was captured on the TL of the LFIA trip in the presence of virus	5 ng mL^{-1}	116
SERS	AdV	Antibody	Ag@Fe_3O_4 NPs functionalized with the antibody and the Raman reporter enriched the virus from impurities by a magnet and was captured on the TL of the LFIA trip	10 PFU mL^{-1}	117
SERS	RSV	Antibody	HRP conjugated antibody in the sandwich complex converted TMB to positive, bound to negatively charged AgNPs	0.05 pg mL^{-1}	118
Fluorometric	CTV	Antibody	Free CTV replaced protein conjugated AuNPs to bind with antibody-conjugated QDs and increased fluorescent signal	0.13 μg mL^{-1}	124
Fluorometric	EV71, CVB3	Antibody	Magnetic nanobeads and QDs functionalized with antibody captured the viruses and exhibited fluorescence signal in positive samples after magnetic separation	1716 copies per mL (EV71);1618 copies per mL (CVB3)	129
Fluorometric	NoV	Antibody	Au/magnetic NPs and QD functionalized with antibody captured the virus and exhibited LSPR-induced fluorescence enhancement in positive samples	0.48 pg mL^{-1}	130
Fluorometric	NoV	Aptamer	Quenched fluorescence was recovered after the release of the 6-FAM labeled aptamer in the presence of the virus	4.4 and 3.3 ng mL^{-1} with MWCNTs and GO	121
Electrical					
Electrochemical	Vaccinia virus	N/A	Carbon nanofiber NEA was able to capture virus and led to impedance changes between NEA and an ITO electrode	~2.58×10^3 particles per mL	145
Electrochemical	ORSV	Antibody	Micro/nano hybrid-structured Au electrodes functionalized with SAM and antibodies targeted virus, leading to EIS responses	0.238 ng mL^{-1}	148
Electrochemical	NoV	Peptide and aptamer	Magnetic nanocomposites modified with aptamer captured by peptide modified electrode in the presence of virus, leading to current change	0.8 copy per mL	152
Electrochemical	NoV	Peptide	WS2NF/AuNP were modified by peptides to capture virus and caused the impedance change	2.37 copies per mL	153
Electrochemical	ALV	Antibody	Fe_3O_4 NPs functionalized with antibody and GOD captured by antibody and β-cyclodextrin-ferrocene functionalized GO platform in the presence of virus, leading to DPV changes	$10^{2.19}$ $TCID_{50}$ mL^{-1}	156
Electrochemical	HCV	Aptamer	CuNPs were synthesized and introduced to rGO when target	405 pM	158

Table 3 *(continued)*

Method	Virus type	Recognition element	General approach	LOD	Ref.
			DNA bound with probe DNA. The electrochemical signal of the oxidation of *o*-phenylenediamine were recorded in the presence CuNPs		
Electrochemical	DENV	Aptamer	ZnO/Pt–Pd modified electrode were functionalized with probe DNA. The electrochemical response of the intercalation of MB and dsDNA were determined	4.3×10^{-5} M	159
Electrochemical	Agrovirus	Aptamer	MWCNTs–CuNPs coated on electrode were functionalized with probe DNA. DPV were determined when viral DNA bound with probe DNA on to reduce MB	0.01 ng μL^{-1}	160
Electrochemical	ZIKV	Antibody	Au array-based electrode functionalized with antibody targeted ZIKV protein, leading to EIS changes	10 pM	164
Chemiresistor	T7, MS2	Antibody	Ppy NWs functionalized with antibodies targeted viruses, leading to NWs resistance changes	10^{-3} PFU	166
Chemiresistor	CMV	Antibody	Ppy nanoribbons functionalized with antibody targeted virus, leading to electrical resistance changes	10 ng mL^{-1}	167
Chemiresistor	DENV	Heparin	SWCNT on electrode was functionalized with heparin. The resistance changed when heparin bound with virus	8.4×10^2 $TCID_{50}$ mL^{-1}	169
FET	EBOV	Antibody	rGO modified FET was functionalized with antibody to target virus. The response was measured by the shift of Dirac voltage	2.4 pg mL^{-1}	178
FET	EBOV	Antibody	FET was modified with rGO, Al_2O_3 and AuNPs and functionalized with antibody. The electronic-resonance frequency was measured	1 ng mL^{-1}	181
FET	EBOV	Antibody	FET was modified with rGO, Al_2O_3 and AuNPs and functionalized with antibody. The electronic-resonance frequency was measured	0.001 mg L^{-1}	183
FET	HBV	Aptamer	ITO NWs functionalized with DNA probe targeted viral DNA, leading to a change in drain current	1 pM	188
Magnetic					
MR	HPV	Aptamer	Streptavidin-coated magnetic NPs were captured by biotin modified target DNA. The changes giant magnetoimpedance were detected	N/A	192
MR	HBV	Aptamer	Streptavidin-coated magnetic NCs were captured by biotin modified target DNA. Magnetic signal was measured	10 copies per mL	193
MRS	HSV, AdV	Antibody	Virus induced antibody functionalized magnetic NPs assembly and resulted in spin–spin relaxation time changes	5 viral particles in 10 μL	199
MRS	NDV	Antibody	Larger magnetic NPs were used to capture virus while smaller magnetic NPs acted as magnetic probes	100 copies per mL	200

dual-modality sensor showed LODs of 0.34 pg mL^{-1} and 4.1 fg mL^{-1} for optical and electrochemical sensing approaches, respectively.

The formation of spherical polydiacetylene (PDA) vesicles through the self-assembly of monomer PDAs can be used for optical virus sensing. Unperturbed PDA vesicles exhibit an intense blue color due to electronic absorption by the conjugated backbone. Virus attachment to PDA vesicles induces backbone distortion, thus resulting in a blue-to-red color change. Using a peptide-functionalized PDA nanosensor for recognizing influenza A virus H1N1, sensitive colorimetric detection was achieved.[87] This peptide has a high affinity against H1N1 viruses compared with others (H3N2, H5N2, and H6N5). When a peptide on a PDA vesicle contacted with the virus, absorbance at 550 (red) and 628 (blue) nm were measured, and the colorimetric responses were calculated based on these changes. The results demonstrated the applicability of the peptide-functionalized PDA nanosensor for the detection of H1N1 with a LOD of 10^5 PFU. In place of the peptide, the antibody conjugated PDA nanosensor has also been coupled with the polyvinylidene difluoride membrane for paper-based virus detection.[88]

In addition to detectable color changes, the absorbance shift of plasmonic nanostructures in the presence of virus can also be recorded by LSPR sensors. Detection sensitivity based upon LSPR shift measurements is dependent on the design and the fabrication of plasmonic nanostructures. An ordered array of triangular Au nanopillars was fabricated for the development of the LSPR sensor based on an octupolar geometry with a minimum interparticle distance between two-unit cells of 25 nm.[89] This interparticle distance produces a non-negligible coupled field between the unit cells and the nanostructure exhibits an absorbance peak in the near-infrared region at 735 nm that undergoes a red-shift when analytes attach and increase the local refractive index. The group found the bulk refractive index sensitivity of the substrate, 280 nm/refractive index unit, was greater than for any previous substrate. The substrate was functionalized with antibody 2B4 for the detection of RV. The optimal antibody concentration (25 μg mL^{-1}) on Au surface attachment was confirmed to obtain a proper configuration with no rotation or deformation and a corresponding higher efficiency for virus trapping. With excess antibody attachment, the access of viruses to the substrate can be sterically inhibited. The

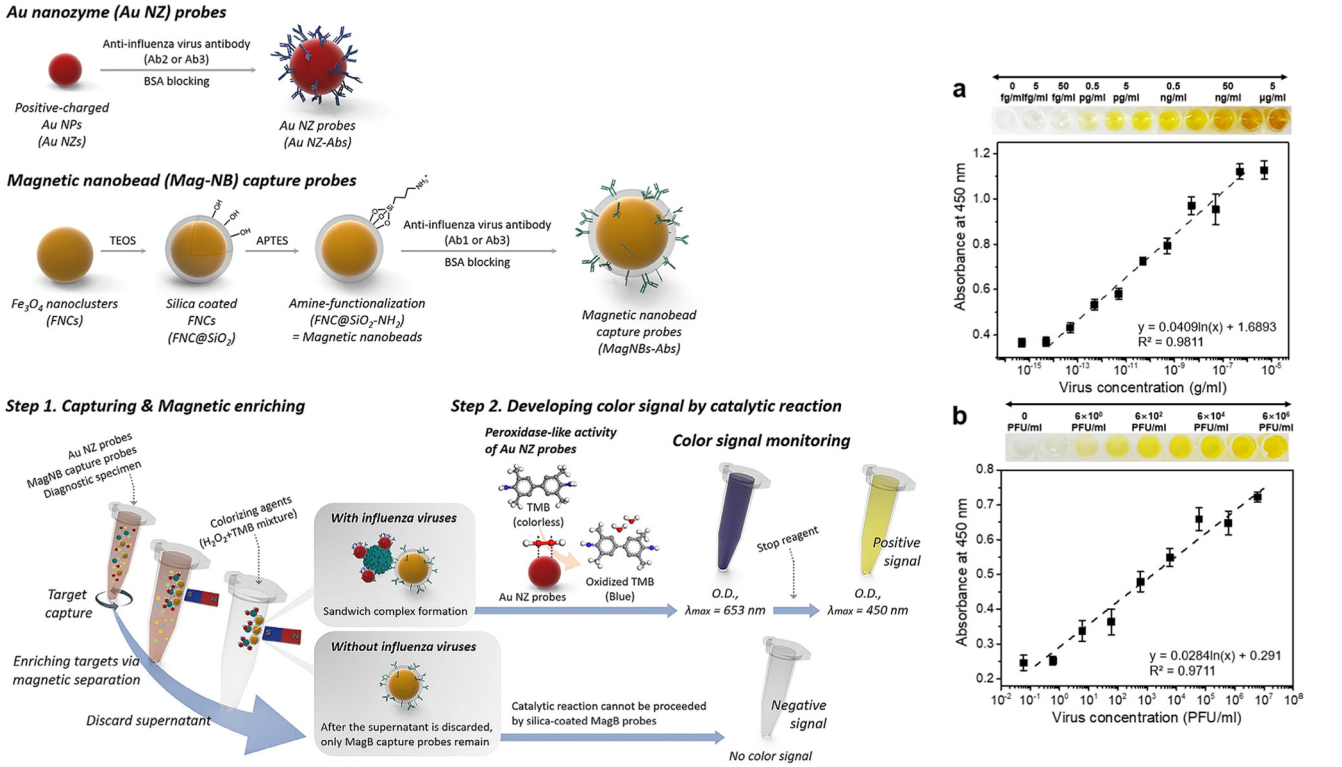

Fig. 2 Colorimetric detection of viruses. Au nanozyme (AuNZ) and magnetic nanoprobe (Mag-NB) were synthesized and functionalized with antibodies to capture the virus and enrich them using a magnetic field. A magnetic nanozyme-linked immunosorbent assay (MagLISA) uses antibody conjugated AuNZs and Mag-NBs to capture the virus and enrich them using a magnetic field. The complexation of virus and AuNZs catalyzes the oxidation of TMB by H_2O_2 and produces a change in color to blue. (a and b) Absorbance at 450 nm and corresponding color change as a function of influenza H1N1 and H3N2 concentration. Adapted with permission from ref. 83. Copyright 2018 American Chemical Society.

LOD of this LSPR nanosensor was estimated to 126 PFU mL^{-1}.

Overall, colorimetric virus detection methods show great sensitivity. Additionally, color changes from virus contact to sensing platforms can be detectable by the naked eye or by cell-phone camera-based methods,[90] enabling straightforward detection without the need for dedicated read-out devices. Hence, we anticipate that research focusing on the simple design of colorimetric assays will be highly advantageous. Furthermore, the insufficient colloidal stability of many colloidal NPs has been found in real samples characterized by macromolecules, natural organic matter, and high ionic can inferfere with detection.[79,91] Stabilizing agents that can resist such interferents should be developed and the applicability of the probes in real environmental samples must be explored.

3.1.2 SERS nanosensors. Raman scattering is the inelastic scattering of a photon that reflects the vibrational transitions of covalent bonds in molecules. Raman spectra represent unique fingerprints of analytes, and the method is becoming increasingly of interest. However, Raman spectroscopy has inherent drawbacks in terms of low sensitivity and high fluorescence interference arising from the weak intensity of inelastic scattering. Since its discovery in the 1970s,[92,93] SERS has greatly expanded the applicability of Raman-based methods across various fields. By electromagnetic (EM) nearfield enhancement of both excitation and inelastic scattering transitions of molecules in hotspots, plasmonic nanomaterials can effectively increase the Raman cross-section of an analyte at their surface vicinity by many order magnitudes.[93] This phenomenon is termed SERS. The sensitivity of SERS is proportional to the density of the EM field. In general, the most enhanced EM fields are found within 10 nm of a plasmonic nanostructure. This region (*i.e.*, referred to as a SERS hot spot) can enhance the Raman signal of an analyte by up to 10^{14}.[94]

The most typical SERS active nanomaterials are Au or AgNPs owing to the tunability of their sizes and shapes and their facile surface functionality.[95] The LSPR frequency of a NP is an important factor that dictates SERS enhancement. The LSPR position can be finely tuned across a wide spectral range by changing the size and shape of plasmonic nanomaterials. For example, the LSPR band of spherical AuNPs with diameters of 10–80 nm ranges from 520–540 nm.[96] The anisotropic shape of Au nanorods (AuNRs) with different aspect ratios results in additional, longer wavelength LSPR positions whose position ranges from 650 to 1050 nm.[96] To achieve the greatest SERS signal, the LSPR of the nanomaterials should spectrally match the excitation laser wavelength.[97] For this reason, the anisotropic shape of AuNRs can support LSPR with intense EM fields (*i.e.*, SERS enhancement) in the NIR region, which is advantageous for

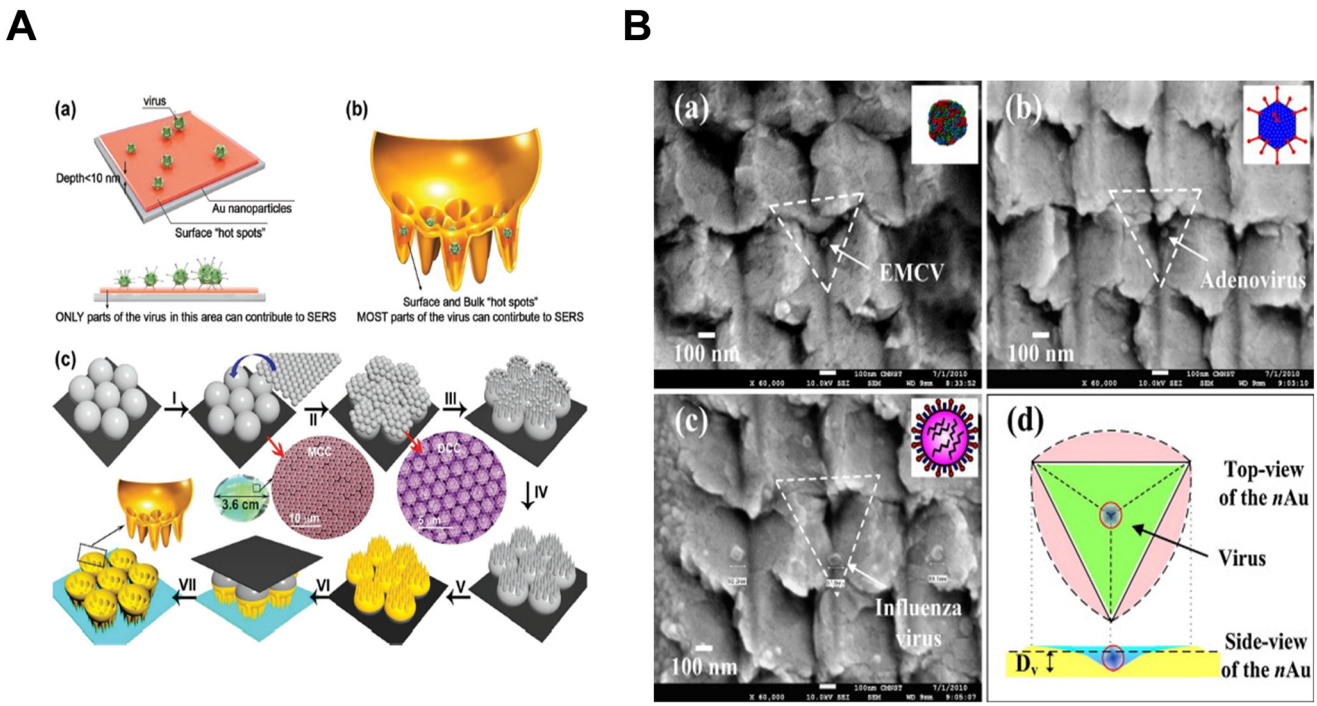

Fig. 3 Fabricated SERS substrates for virus detection. (A) Au hollow nano-cone-shaped SERS substrate with indentations for sensitive SERS hot spots inspired by "molecular printing". (a) Conventional SERS substrates (b and c) a hollow nano-cone-shaped virus-targeting SERS substrate and its fabrication process. Adapted with permission from ref. 100. Copyright 2019 Wiley-VCH. (B) Inverted triangular Au nano-cavity arrays with different sizes for (a) EMCV, (b) AdV, and (c) influenza virus H1N1. (d) The dimension of virus with respect to top- and side-views of the SERS substrates. Adapted with permission from ref. 102. Copyright 2011 Elsevier B. V.

allowing SERS measurements with NIR laser excitation (*i.e.*, 785 nm) to minimize autofluorescence background.

SERS can be classified as labeled or label-free methods based on the molecular source of the Raman signal. Label-free SERS reflects the intrinsic signals arising from the virus itself. On the other hand, labeled methods rely upon Raman reporters (*e.g.*, malachite green isothiocyanate (MGITC), rhodamine B isothiocyanate (RBITC), 4-aminothiophenol (4-ATP)) that have large Raman cross-sections and high affinity to the plasmonic nanomaterial surface. The specific interaction among platform, targeted virus, and labeled nanomaterials induces SERS readout changes of Raman reporter on developed platform.

Luo *et al.* synthesized porous carbon film-coated AgNPs as SERS substrates for label-free detection of porcine circovirus type 2 (PCV2), porcine parvovirus (PPV), and porcine pseudorabies virus (PRV).[98] The porous structure and hydrophobicity of the substrates can increase viral adsorption and facilitate recyclability. Caglayan *et al.* synthesized AuNR-based SERS substrates to detect potato virus X (PVX).[99] To enable SERS-based virus detection, the SERS hot spot size should be carefully considered. The relatively large size of intact viruses (~100 nm) makes them difficult to deposit within nanometer-sized SERS hot spots. Recently, a hollow nano-cone-shaped virus-targeting SERS substrate was fabricated by "molecular imprinting" (Fig. 3A).[100] The ~100 nm opening of the hollow nano-cone can accommodate a range of virus sizes (*e.g.*, adenovirus type 5 (Ad5), 60–90 nm; coxsackievirus type 3 (Cv3), 22–30 nm) while simultaneously possessing a high density of hot spots due to the 3D configuration. The authors' termed the approach volume-enhanced Raman scattering (VERS) and achieved reproducible and reliable detection of Ad5 and Cv3. Durmanov *et al.* synthesized porous Au nanofilms by electron beam physical vapor deposition and used them for the detection of rabbit myxomatosis virus (MYXV), canine distemper virus (CDV), tobacco mosaic virus (TMV), and PVX.[101] The structure of the synthesized substrate has ~300 nm pore-like nano-cavities and indentations that allow for target virus (100–300 nm) capture in the vicinity of the SERS hot spots. Target viruses were successfully detected using this SERS substrate without any recognition elements and differentiated by linear discriminant analysis (LDA). Chang *et al.* fabricated inverted triangular Au nano-cavities with various indentation depths to entrap AdV, influenza A virus H1N1, and *Encephalomyocarditis* virus (EMCV) (Fig. 3B).[102] Different sizes and nano-cavity dimensions were fabricated and tested with the three viruses. The substrate with a matching cavity entrapment size to the viruses successfully entrapped them into nano-cavities and induced their SERS spectra. Using the best-fitting SERS substrate, the detectable concentration for AdV and EMCV was 10^6 PFU mL^{-1}, while for H1N1 it was 10^4 PFU mL^{-1}.

To capture specific viruses, plasmonic nanomaterials can be functionalized with recognition elements such as aptamers, antibodies, peptides, and chemical molecules. Recently, cell receptor angiotensin-converting enzyme 2 (ACE2) has been used as a recognition element for SARS-CoV-

2 owing to its high affinity to spike protein receptor-binding domain (S RBD). Yang *et al.* fabricated ACE2-functionalized gold nanoneedles for selective capture and SERS detection of SARS-CoV-2. This platform exhibited a LOD of 80 copies per mL.[103] Similarly, Ag nanorods (AgNRs) functionalized with ACE2 enabled rapid SERS detection of SARS-CoV-2 in environmental specimens.[104] In this result, SERS peaks arising from ACE2 were quenched by hydrophilic interaction at ACE2/RBD when SARS-CoV-2 spike protein bound to the substrates.

The specific interaction and high equilibrium association constants for the antibody–antigen complex enhance sensitivity and specificity.[105] Moon *et al.* synthesized antibody conjugated AuNPs using a gold binding peptide (GBP) and used them for labeled SERS detection of influenza A virus H1N1.[106] GBP can be attached to the surface of AuNP and the Fc (Fragment, crystallizable) region of an antibody. The target virus was selectively captured on an antibody-conjugated glass slide. Detection was then enabled by the attachment of RBITC functionalized AuNPs with the Raman signal of RBITC used to indicate virus detection. The sensitivity of this substrate was improved to a LOD of 4.1×10^3 TCID mL^{-1} by adding a signal-enhancing Ag layer. Using the same principle, a two-dimensional Au@Ag core–shell NP array was synthesized as a SERS substrate for sensitive detection of influenza A virus nucleoprotein.[107] The SERS signal of this array was ~4× greater than that of a flat Au film. Sandwich formation with 4,4′-thiobisbenzenethiol-coated AuNPs in the presence of influenza A virus nucleoprotein showed a LOD of 6 $TCID_{50}$ mL^{-1}.

Recently, oseltamivir hexylthiol (OHT) and MGITC functionalized AuNPs were utilized for SERS detection of oseltamivir-resistant virus.[108] The wide use of oseltamivir (Tamiflu) to prevent influenza virus infection has led to the emergence of oseltamivir-resistant virus strains. It was found that OHT exhibited a higher affinity for oseltamivir-resistant (pH1N1/H275Y mutant) viruses than for the wild-type virus.[109] Using MGITC functionalized AuNPs, pH1N1/H275Y mutant viruses were successfully detected due to the SERS MGITC signal enhancement that occurs from analyte-mediated AuNP aggregation. Even with the high concentration of wild-type viruses, the functionalized AuNPs were able to selectively detect pH1N1/H275Y mutant viruses. Moreover, these functionalized AuNPs can be used for mutant virus diagnosis in complex nasal fluid and saliva specimens with concentrations as low as 1 PFU.[110]

Aptamer-functionalized SERS substrates can also be utilized to selectively detect the virus. Recently, Chen *et al.* synthesized DNA aptamer functionalized Au nanopopcorn with high affinity to the spike protein of SARS-CoV-2.[111] A Raman reporter, cyanine 3 (Cy3), was attached to the aptamer and situated close to the surface of the substrate. The aptamer was designed to be released when it binds to the spike protein of SARS-CoV-2. The release of aptamer from the substrate then leads to a decrease in the Cy3 Raman signal. This platform successfully detected SARS-CoV-2 lysate with a LOD of <10 PFU mL^{-1} within 15 min. Aptamer RHA 0385 showed a high affinity for influenza A viruses of the H1N1, H3N2, and H5N1 strains.[112] For the detection of influenza viruses, the SERS substrate was synthesized by covering a thick layer of Ag granules on a silicon plate.[113] A SERS substrate functionalized with primary aptamer (RHA 0385) was used to capture the virus. Following capture, the secondary aptamer, Cy3 labeled RHA 0385, formed a sandwich complex in the presence of the influenza virus. The high Raman signal of Cy3 enabled sensitive viral detection.

For simple point-of-care (POC) or point-of-use (POU) virus detection, a SERS-based lateral flow (LF) strip has proven effective.[114–117] LF strips are an attractive sensor platform that relies upon capillary force-driven sample movement through a stationary membrane. Traditionally, targeted analytes can be captured by immobilized recognition elements and detected by the visual color of colloidal samples such as AuNPs. SERS-based LF strips can selectively capture analytes with high sensitivity and easy operation.[114] Xiao *et al.* synthesized novel core–shell structured plasmonic NPs ($AuAg^{4\text{-}ATP}$@AgNPs) consisting of a double-layered shell of Au and Ag and an AgNP core that was functionalized with 4-ATP as a Raman reporter.[115] To capture influenza A virus H7N9, a H7N9 monoclonal antibody was conjugated to the $AuAg^{4\text{-}ATP}$@AgNPs and the test line (TL) on the strip while goat anti-mouse IgG was used for the control line (CL). High sensitivity detection of H7N9 was achieved using these SERS-based LF strips with a LOD of 0.0018 hemagglutination unit (HAU). Using the same method, selective and sensitive detection of PRV was realized with a detection limit of 5 ng mL^{-1}.[116] Further, a magnetic SERS-based LF strip was developed to detect influenza A virus H1N1 and AdV in biological samples.[117] Magnetic NPs have the advantage of facile magnetic enrichment and the separation of target viruses from potentially interferent constituents without pretreatment. Wang *et al.* synthesized iron oxide and Ag core–shell NPs (Fe_3O_4@AgNPs) for such a SERS application (Fig. 4).[117] Fe_3O_4@AgNPs were functionalized with 5,5-dithiobis-(2-nitrobenzoic acid) as a Raman reporter, and two specific antibodies to H1N1 and AdV were conjugated to the particles. Fe_3O_4@Ag NPs were incubated in H1N1- and AdV-spiked human whole blood, serum, and sputum. The conjugates were then magnetically separated and re-suspended in the buffer for SERS/LF strip-based detection. Two separate test lines for H1N1 and AdV each with virus specific antibodies were used. Upon addition of suspension onto the LF strip, the two test lines are positive in the presence of each virus. The LODs were 50 and 10 PFU mL^{-1} for H1N1 and AdV, respectively. The stability of the platform was tested in 0.1 M PBS over a pH range of 5.0–9.0. There was no significant effect of pH on detection performance.

SERS was recently coupled with an enzyme-catalyzed immunoassay for virus detection. In the presence of the target virus, an enzyme reaction product induces NP aggregation and facilitates the generation of a strong SERS signal. Zhan *et al.* detected respiratory syncytial virus (RSV)

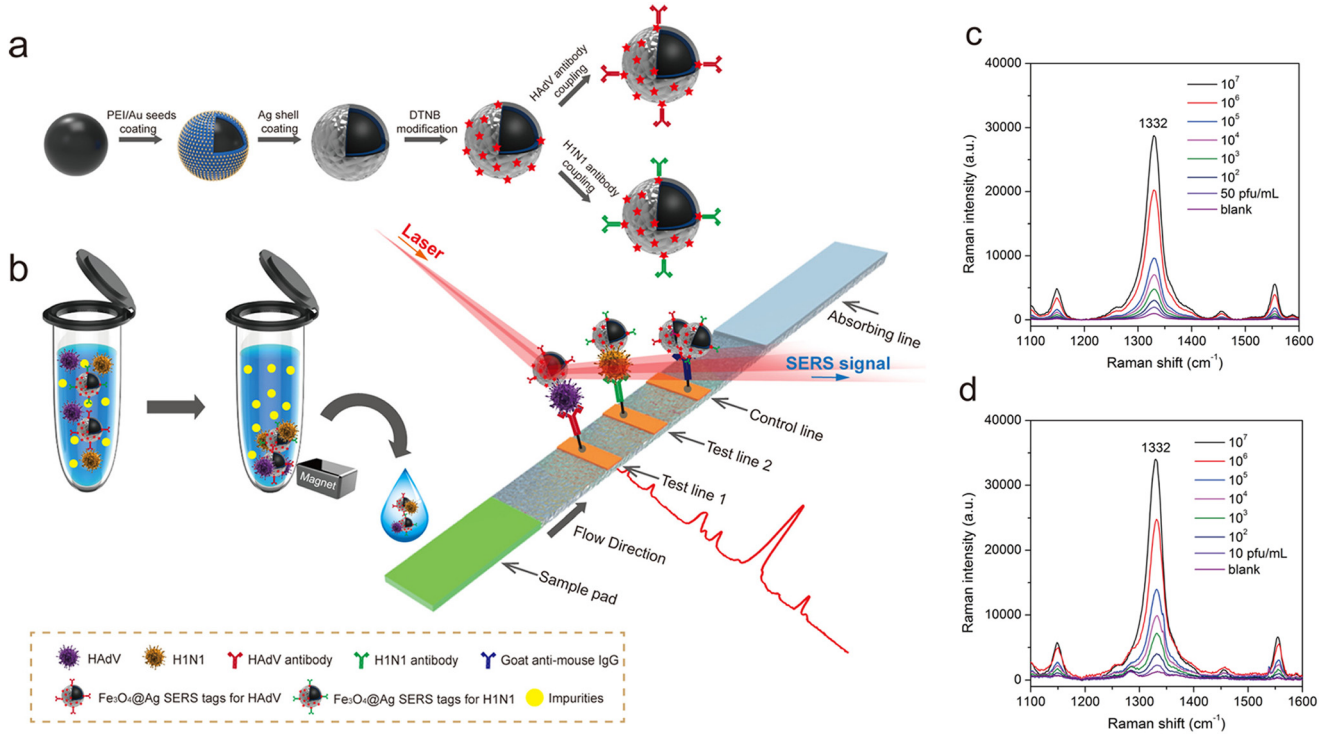

Fig. 4 SERS detection of viruses. (a) Two antibody-conjugated Fe_3O_4@Ag core–shell NPs were synthesized for the detection of H1N1 and AdV. (b) Dual SERS detection was enabled by a magnetic SERS-based LF strip. H1N1 and AdV were selectively separated from impurities *via* a magnetic field. (c and d) SERS spectra of test lines 1 and 2 with different concentrations of H1N1 and AdV. Adapted with permission from ref. 117. Copyright 2019 American Chemical Society.

using an HRP-induced catalytic reaction and SERS. HRP catalyzes the oxidation of TMB by H_2O_2 to TMB^+.[118] Through constructing a sandwich complex between HRP conjugated antibody and RSV, TMB was converted into a positively charged reactant that electrostatically binds to the negatively charged AgNPs. Following complex formation, AgNP aggregation produced strong SERS signals for oxidized TMB. The LOD of this method was 0.05 pg mL^{-1}.

Overall, both label-free and labeled SERS show great potential for sensitive virus detection. Label-free SERS reflects the intrinsic signal of the virus itself but exhibits lower sensitivity. We anticipate that virus size-oriented design of label-free SERS substrates that enable effective deposition of the virus within dense SERS hot-spots will be of growing research focus as a means to increase SERS intensity. Moreover, advanced data analytics should help virus discrimination and quantification in more complex systems.[119] Labeled SERS takes advantage of the strong signal of Raman reporter molecules, but requires an additional surface functionalization process. Different Raman reporters and recognition elements should be modified for the detection of multiple viruses.[117] Raman instrumentation can be costly in a bench-top format. However, there are a field-deployable formats (*i.e.*, portable Raman instruments) that come with great mobility and lower prices. In addition, it is relatively simpler to operate than current PCR-based assays since it does not require any reagents to run the assay. It would essentially reduce the cost of maintenance and analysis. In future studies, the expansion of multiplex labeling should be improved. In addition, SERS has exhibited great compatibility with POC/POU platforms such as LF. The stability of SERS substrates for real sample applications and the costs should be considered in future studies.

3.1.3 Fluorometric nanosensors. Fluorescent nanomaterials can induce down-conversion or up-conversion fluorescence emission, mediated by single-photon or multi-photon excitation and emission transitions between their electronic states. Therefore, fluorescent nanomaterials can be engineered as fluorometric nanosensors or nanoprobes to detect viruses or other bio-markers based on their interfacial interaction-modulated fluorescence emission signal changes.[120] For example, fluorescence can be quenched when an analyte attaches to a fluorescent NP and disrupts the non-radiative transfer of energy, referred to as fluorescence resonance electron transfer (FRET). On the other hand, the interaction between the analyte and the fluorescent NPs can enhance fluorescence emission by minimizing the quenching pathway associated with the surrounding environment. Fluorescent single isomers such as 6-carboxylfluorescein (6-FAM) can be coupled with NPs to develop fluorometric nanosensors.[121] Recently, single-walled CNT (SWCNT) fluorometric nanosensors were developed for SARS-CoV-2 detection.[122] The SWCNTs were functionalized with ACE2 for high affinity to SARS-CoV-2 spike protein, leading to fluorescence quenching. The presence of

SARS-CoV-2 S RBD resulted in an increase in prequenched fluorescence within 90 min with a LOD of 12.6 nM.

The LSPR of plasmonic NPs can be applied to fluorometric virus sensing approaches. Fluorescence signal intensity can be controlled by coupling plasmonic NPs to fluorescent particles.[123] Numerous FRET-based sensors have been developed for virus detection. Shojaei *et al.* detected citrus tristeza virus (CTV) using CdTe QDs coupled with AuNPs.[124] Formation of an immuno-complex between CTV protein conjugated AuNPs and antibody-conjugated QDs that have a high affinity to CTV protein quenched the fluorescent signal. By competitively replacing AuNPs with free CTV protein in the presence of CTV, the fluorescent signal increased. The authors found that an AuNP and QD molar ratio of 1 : 6.5–8.5 showed the highest FRET efficiency. The detection assay showed a LOD of 0.13 μg mL^{-1}. Takemura *et al.* also applied the LSPR from AuNPs to enhance fluorescence from quaternary alloy CdSeTeS QDs.[125] *Via* the same antigen–antibody interaction, AuNPs and QDs were attached to influenza A virus H1N1. LSPR-induced immunofluorescence enhancement was ~3.6 fold compared to QDs alone and enabled sensitive detection of H1N1 with a LOD of 0.03 and 0.4 pg mL^{-1} in deionized water and human serum, respectively. In addition to AuNPs, CNTs combined with AuNPs have a synergistic effect on fluorescence enhancement.[126] Au-Decorated CNTs (AuCNTs) exhibit a unique platform to work as a combined signal enhancer and transducer. Using antibody conjugated AuCNTs and CdTe QDs as a plasmon-assisted fluoro-immunoassay (PAFI) platform, influenza A H1N1 and H3N2 viruses were detected. The minimum detection concentration was 0.1 pg mL^{-1}. For the clinically isolated viruses, the LOD was 50 PFU mL^{-1}.

Many studies have employed plasmonic NPs with LSPR to control the intensity of the fluorescent signal. The enhancement of fluorescence signals by such plasmonic NPs highly depends on the distance between the plasmonic NPs and QDs. It has been observed that fluorescence can be enhanced at a distance of 10–15 nm between them and can be quenched at a distance of <5 nm.[127] Using the principle of fluorescence quenching by steric hindrance between fluorescent and plasmonic NPs, a highly sensitive virus detection biosensor was developed (Fig. 5A).[128] Fluorescent inorganic QDs (CdZnSeS/ZnSeS QDs) and AuNPs were linked by an 18 amino acid peptide chain. This peptide was functionalized with specific antibodies against influenza A virus H1N1. Following virus attachment to the peptide chain linker between the QDs and AuNPs, the fluorescence intensity was gradually quenched. This tunable LSPR-assisted fluorometric detection approach achieved a detection limit of 17.02 fg mL^{-1}.

Many biological samples contain impurities that may deteriorate detection efficiency or impede fluorescence emission, resulting in unreliable results. Magnetic NPs can be applied to separate the analyte from impurities in the sample using an external magnetic field. Multiplex detection of EV71 and coxsackievirus B3 (CVB3) using antibody-conjugated magnetic nanobeads and CdSe QDs was successfully used for clinical swab samples.[129] Two specific antibodies to EV71 and CVB3 were used to functionalize the magnetic nanobeads and two colored QDs with different emission wavelengths (QDs 525 and 605) were employed. With both viruses present, strong fluorescence signals from QDs 525 and 605 were simultaneously observed with LODs of 858 and 809 copies/500 μL for EV71 and CVB3, respectively.

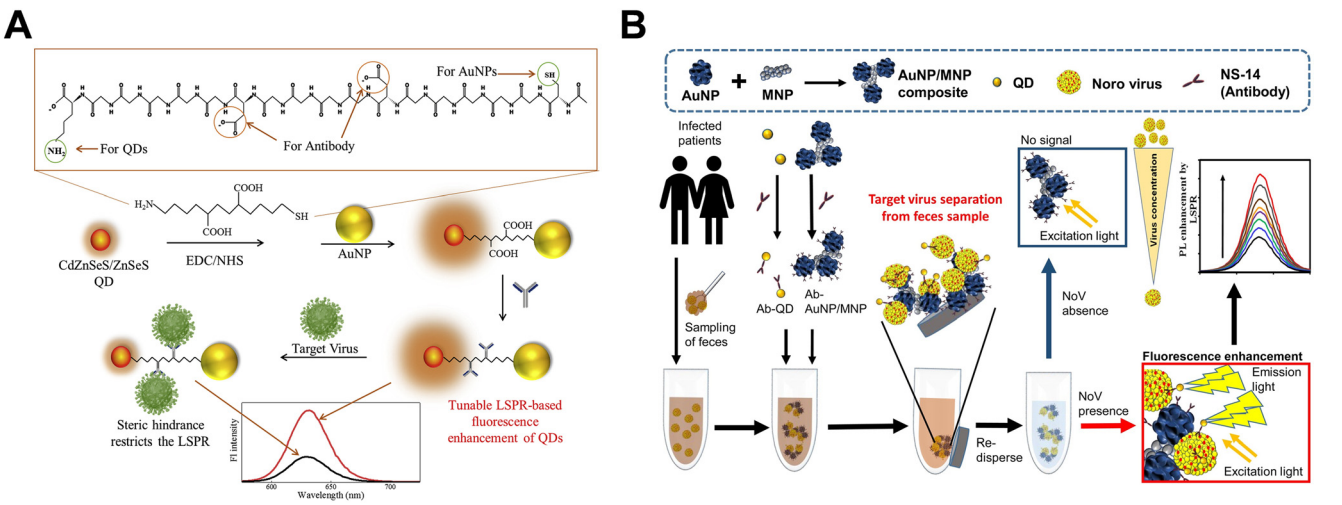

Fig. 5 Fluorometric detection of viruses. (A) AuNPs and QDs were linked through the peptide chain to induce tunable LSPR-based fluorescence enhancement of QDs. The peptide chain was functionalized with the antibody and fluorescence was quenched by steric hindrance when the target virus was attached to this chain. Adapted with permission from ref. 128. Copyright 2020 Elsevier B. V. (B) LSPR-amplified magnetofluoroimmunoassay (MFIA) was used for the detection of NoV separated from human feces. Au/magnetic NPs (AuNP/MNP composite) and QDs were functionalized with antibodies to capture NoV. Complexes of NoV-captured AuNP/MNP composite and QDs were separated from human feces and enriched by a magnetic field. The concentration of NoV was reflected by fluorescence enhancement. Adapted with permission from ref. 130. Copyright 2019 Elsevier B. V.

Using Au and magnetic hybrid NPs coupled with QDs, a LSPR-amplified magnetofluoroimmunoassay (MFIA) for detecting NoV was reported (Fig. 5B).[130] Hybrid NPs conjugated with antibodies that have a high affinity to NoV enabled virus capture from human feces. Complexes of NoV-captured hybrid NPs and antibody conjugated L-glutathione-capped CdSeS core QDs were successfully separated from human feces by a magnetic field. This approach provided an LSPR-amplified fluorescence signal only in the presence of NoV with a LOD of 0.48 pg mL^{-1}.

For simplicity and rapid detection, a fluorescent immunochromatographic strip test (FICT) assay has been developed. The strip assay uses capillary forces, as previously described, to move the sample through a stationary membrane. At the TL and CL, anti-virus antibodies and anti-mouse immunoglobulin are conjugated. At the TL, in the presence of a target virus, fluorescent NPs conjugated with anti-virus antibodies form a sandwich complex with the virus and the fluorescence intensity at the TL and CL were measured, and the TL/CL ratio was used for quantitative analysis. Recently, FICT assays were developed for influenza A virus H1N1-confirmed patients.[131,132] Using commercially available Europium NPs, the reported LOD of the assay was below 20 HAU mL^{-1}. The assay also showed 85.3% sensitivity and 100% specificity for patient diagnosis. Antibodies to influenza H7 subtype virus were developed for better selectivity and used for detecting H7N1 and H7N7.[133] The FICT assay was only positive for H7N1 and H7N7 with a LOD of 40 HAU mL^{-1} and was negative for H1N1 and H5N3. Additionally, to improve the system detection sensitivity, CdSe/CdS/ZnS QDs were applied instead of Europium NPs. The QDs were functionalized with 3-mercaptopropionic acid to make them water-soluble. The higher quantum yield and fluorescence efficiency of CdSe/CdS/ZnS QDs-linked FICT assay showed lower LODs (2.5 HAU mL^{-1} for H1N1 virus and 0.63 HAU mL^{-1} for H3N2 virus).[132]

Aptamer functionalized QDs have also been used for virus detection. A QD embedded target-responsive hydrogel sensor functionalized with aptamer was developed to detect influenza A virus H5N1.[134] Polymer crosslinked aptamer hydrogel with a high affinity to H5N1 surface hemagglutinin was synthesized and terminated with QD quenchers. The hydrogel protects the QDs from external interference. Using single-strand DNA (ssDNA) terminated QDs, H5N1 was detected through the interaction between aptamer–quencher and ssDNA–QD. In the presence of H5N1, aptamer was attached to the virus and the fluorescence signal was observed from ssDNA–QD. This method showed the lowest detection limit of 0.4 HAU. Weng and Neethirajan reported the detection of NoV enabled by aptamer functionalized 6-FAM coupled with multi-walled CNTs (MWCNTs) or GO.[121] Carbon-based nanomaterials were used as fluorescence quenchers of FRET. When 6-FAM terminated aptamer with high affinity to NoV was bound with MWCNTs or GO in the absence of NoV, the fluorescence signal was quenched. The aptamer can be released when it binds to NoV, leading to fluorescence recovery. The reported LODs were 4.4 and 3.3 ng mL^{-1} when MWCNTs and GO were used, respectively.

The surveyed literature suggests that fluorometric nanosensors can successfully detect viruses. We anticipate that a growing number of nanomaterials that can effectively quench fluorescence signals or improve FRET efficiency will be developed. Additionally, due to the low quantum yield and photobleaching issue of some fluorescent NPs, the search of synthesis of low-cost, stable, and efficient nanomaterials is an ongoing area of research focus.[135–138]

3.2 Electrical nanosensors

Electrical nanosensors employ conductive nanomaterials such as carbon-based materials (*e.g.*, CNTs and graphene), metals, and metal oxides (*e.g.*, titanium oxide (TiO_2), zinc oxide (ZnO)), polymers, and other inorganic nanomaterials,[139–141] as the signal transducer to convert interfacial analyte binding events into electrical voltage or current signals. According to the underlying signal transduction mechanisms, electrical nanosensors can be primarily classified into electrochemical nanosensors, chemiresistor-based nanosensors, and field-effect transistor based nanosensors.[141]

3.2.1 Electrochemical nanosensors. As a prominent type of electrical nanosensors for virus detection, electrochemical nanosensors exploit the highly sensitive dependence of interfacial electrochemical processes on the analyte binding events at the nanomaterials-modified microelectrode surface for signal transduction. Electrochemical sensors are suitable for real-time virus detection because they can potentially achieve high sensitivity, good selectivity, low-device cost, compact instrumentation, high portability, and fast analysis.[142]

To date, electrochemical nanosensors primarily utilize carbon-based nanomaterials[143] and metal/metal oxide NPs.[144] Usually, these nanomaterials are used to modify electrodes for better capture of the target virus and for the amplification of the transductor signal. The most straightforward approach for virus detection using electrochemical nanosensors is the direct capture of viruses on the electrode surface and the subsequent measurement of electrical signal changes. Employing an embedded vertically aligned carbon nanofiber nanoelectrode array (NEA), Madiyar *et al.* captured vaccinia virus particles and measured virus concentration based on the electrochemical signal change (Fig. 6A).[145] The virus particles were first captured by the NEA using a low voltage and the interfacial impedance changes at the electrode were subsequently measured. A LOD of $\sim 2.58 \times 10^3$ particles per mL was reported. This rapid, reversible, and label-free detection method exhibited potential for future study. In addition to pre-immobilizing nanomaterials on the electrode, we can simultaneously introduce the NPs and the virus analytes to the sensor surface to improve detection performance. Sepunaru *et al.* found that in the presence of the influenza virus, AgNPs can be adsorbed on a carbon

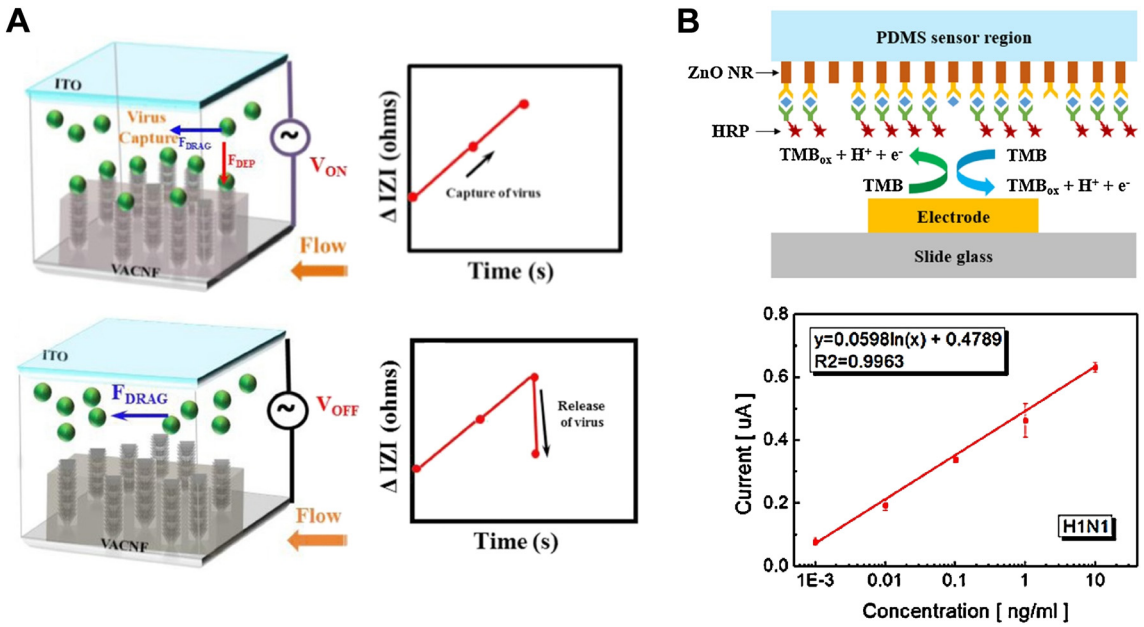

Fig. 6 Electrochemical detection of viruses. (A) Direct virus particle capture using carbon nanoelectrode arrays when the voltage is on and off. Adapted with permission from ref. 145. Copyright 2017 Wiley-VCH. (B) TMB–HRP oxidation mechanism on the electrochemical immunosensor working electrode and the calibration curve of the H1N1 sensor at different concentrations. Adapted with permission from ref. 150. Copyright 2016 Elsevier B.V.

electrode efficiently at open circuit potential due to the 'sticky' property of the H1N1, which comes from the adsorption of viral proteins to electrode surface.[146] The frequency and amplitude of the current spikes showed a high linear correlation with virus concentration. This method enabled rapid detection of influenza virus H1N1 at the sub pM level.

Unfortunately, direct viral capture methods cannot ensure specific binding of the target virus and changes in the electrochemical signal are not always strong enough to be detectable. For these issues, recognition elements can be used to modify the electrode surface.[147] Antibodies are the most commonly used recognition elements for this purpose. To date, many researchers have adapted antibody-modified electrochemical biosensors for virus detection.[148,149] Wang *et al.* fabricated AuNP-based micro/nano hybrid-structured sensing electrodes to detect *Odontoglossum* ringspot virus (ORSV).[148] The electrodes were first modified with a self-assembled monolayer (SAM) of anti-ORSV antibodies and electrochemical impedance spectroscopy (EIS) changes were monitored for ORSV quantification. This method has achieved a low LOD (0.238 ng ml^{-1}). Similarly, a microfluidic immunosensor has been successfully developed for simultaneous sensing of influenza A virus H1N1, H5N1, and H7N9 (Fig. 6B).[150] ZnO nanorods (ZnONRs) on the polydimethylsiloxane surface in the sensing region enhanced the sensitivity of the amperometric signal and the LOD was as low as 1 pg mL^{-1} for each virus. Recently, Hashemi *et al.* developed an electrochemical diagnostic kit by coating a layer of GO with sensitive chemical compounds (8-hydroxyquinoline, 1-ethyl-3-(3-dimethylaminopropyl)carbodiimide (EDC), and *N*-hydroxysuccinimide (NHS)) along with gold nanostars (AuNSs).[151] Differentiable fingerprint DPV patterns of SARS-CoV-2 and animal virus glycoproteins can be obtained at different voltage positions. The sensor demonstrated a LOD of 1.68×10^{-22} μg mL^{-1} toward SARS-CoV-2 in biological media. Peptides are another commonly used recognition element in electrochemical sensors for virus detection. Zhao *et al.* developed a sandwich type electrochemical sensor for NoV using both aptamer and peptide recognition elements.[152] Aptamer was modified on magnetic nanocomposites while peptides were functionalized on the surface of an AuNP modified electrode. The sensor showed high sensitivity with a LOD of 0.8 copy per mL. Baek *et al.* developed a peptide functionalized electrochemical sensing platform for NoV.[153] AuNP-decorated tungsten disulfide nanoflowers (WS2NF/AuNP) were modified by peptides and specifically capture NoV. The impedance is increased through hindrance of charge transfer between the working electrode and redox species with a LOD of 2.37 copies per mL.

To enhance the electrochemical signal, labels (primarily enzymes) have been used to produce or consume an electroactive cofactor that can be monitored at the electrode interface.[105] HRP is a commonly used enzyme label in electrochemical sensors. HRP conjugated antibodies are attracted to the electrode surface in the presence of viruses. TMB on the surface of the electrode can be oxidized by HRP, resulting in an electrochemical redox current (Fig. 6B).[150] Glucose oxidase (GOD) and alkaline phosphatase are two other frequently used enzyme labels.[154,155] Conjugated GOD is an extraordinary electrochemical biocatalyst for the reduction of ionic β-cyclodextrin-ferrocene and has been

successfully applied to detect avian leukosis virus (ALV).[156] In addition to redox labels, electrochemiluminescence (ECL) labels are also commonly used for virus detection.[157] Luo *et al.* successfully detected influenza A virus H9N2 by encapsulating $Ru(bpy)_3^{2+}$ in silica nanoparticles (RuSi NPs) and then modifying these NPs with a polyclonal antibody.[157] The ECL signals were amplified about 10^3-fold compared with the same concentration of $Ru(bpy)_3^{2+}$. Antibody-modified magnetic nanobeads were used to capture and separate virus conjugated RuSi NPs and the ECL immunosensor achieved ultrasensitive detection of 14 fg mL^{-1} for H9N2. Combinations of labels and nanomaterials can significantly improve detection sensitivity.

To expand the application of electrical nanosensors for virus detection, some researchers have focused more on sensing viral nucleic acid (DNA or RNA) than intact viruses. Electrochemical DNA/RNA sensing techniques can be used for virus identification and quantification with high sensitivity and specificity. Often, ssDNA sequences and different kinds of indicators are modified on nanomaterials adhered to the electrode surface.[158,159] When a complementary target sequence approaches, the redox reaction on the indicators will cause the change in the electrochemical signal and the target viral sequence can be detected. Tahir *et al.* successfully detected agrovirus DNA in infected plant leaves using methylene blue (MB) as a redox indicator.[160] CNT-based copper NP composites were used to immobilize probe DNA. When DNA hybridization happened, the electroactivity of MB solution decreased and the reduction in current was used for quantification. Li *et al.* developed a DNA-assisted magnetic reduced graphene oxide (mrGO)–copper nanocomposite (CuNCs) for the detection of hepatitis C virus (HCV).[158] CuNCs combine with mrGO when probe ssDNA hybridized with target HCV DNA. The indicator, *o*-phenylenediamine, is oxidized to 2,3-diaminobenazine in the presence of CuNCs and the electrochemical signal is used to characterize the HCV DNA.

Nucleic acid-based methods have been also successfully used for SARS-CoV-2 detection. Alafeef *et al.* developed an electrochemical biosensor using AuNPs functionalized with ssDNA to target SARS-CoV-2 RNA.[161] The sensor provided a significant increase in output signal only in the presence of SARS-CoV-2 RNA within <5 min and the LOD was 6.9 copies per μL. Using a similar principle, Zhao *et al.* developed a rapid, accurate, and easy-to-implement electrochemical sensor for SARS-CoV-2 RNA diagnosis.[162] When applied to a clinical specimen, the LOD was 200 copies per mL and the detectable ratios for SARS-CoV-2 confirmed patients were even higher than those obtained using RT-qPCR. More recently, Chaibun *et al.* applied such a sandwich assay for SARS-CoV-2 amplicons from rolling circle amplification.[163] The probes were functionalized with redox-active labels. The one-step sandwich hybridization assay could detect as low as 1 copy per μL of genes within 2 h. The developed sensor gave a 100% concordance result with PCR-based technique when evaluating 106 clinical samples. In addition to nucleic acid, the other components of viruses such as proteins[164] and peptides,[165] can also be detected using similar methods. For example, Kaushik *et al.* developed a functionalized interdigitated micro-electrode Au array for ZIKV protein detection.[164] The ZIKV protein could bind with ZIKV-specific envelop protein antibody, and EIS was used to measure the electrical impedance responses of the developed sensing chip with a LOD of 10 pM. The detection of nucleic acid and protein greatly expanded the applicability of virus detection through electrochemical nanosensors.

3.2.2 Chemiresistor-based nanosensors. Chemiresistors-based nanosensors employ nanomaterials with chemosensitive resistance to convert analyte adsorption–desorption events at the sensor surface into sensor resistance changes for electrical signal readout. In this way, chemiresistor nanosensors can detect viral analytes in real-time.

One-dimensional nanostructures such as SiNWs, conducting polymer NWs, and CNTs are the most often used nanomaterials in chemiresistors.[141] When used for virus detection, recognition elements are essential for most chemiresistors since viruses alone seldom change the resistance without a recognition element. Like other types of nanosensors we discussed earlier, antibodies are the most often used recognition elements in chemiresistors. Shirale *et al.* developed chemiresistive immunosensors based on single polypyrrole (Ppy) NWs to detect bacteriophages T7 and MS2 through immobilization of anti-T7 or anti-MS2 antibodies (Fig. 7A).[166] Ppy NWs were used to connect a pair of Au electrodes and modified with different antibodies. A change in sensor resistance was observed upon exposure to different concentrations of spiked bacteriophages and the LOD reached 10^{-3} PFU in 10 mM PBS for both targets. Cucumber mosaic virus (CMV) can be detected *via* similar approach.[167] However, antibodies are sensitive to environmental condition changes (such as pH, temperature, enzymes, and other substances) and may not be applicable for biosensing under field conditions.[168] Hence, some researchers have used other recognition elements in chemiresistors. Wasik *et al.* developed a heparin-functionalized CNT-based chemiresistor for DENV.[169] In their study, they used heparin as the recognition element since it is stable during storage under adverse conditions. In the presence of heparin, DENV could be captured on the surface of CNT and elicited an increase in resistance.

Nucleic acid can also be used to determine viruses in chemiresistors. Prior studies have found that DNA probe can be non-covalently attached to CNT sidewalls due to their strong van der Waals attraction to hexagonal carbon structures.[170] Fu *et al.* developed a chemiresistor based on CNTs to detect the DNA sequence of influenza A virus H5N1 (Fig. 7B).[171] In this biosensor, the CNTs were first

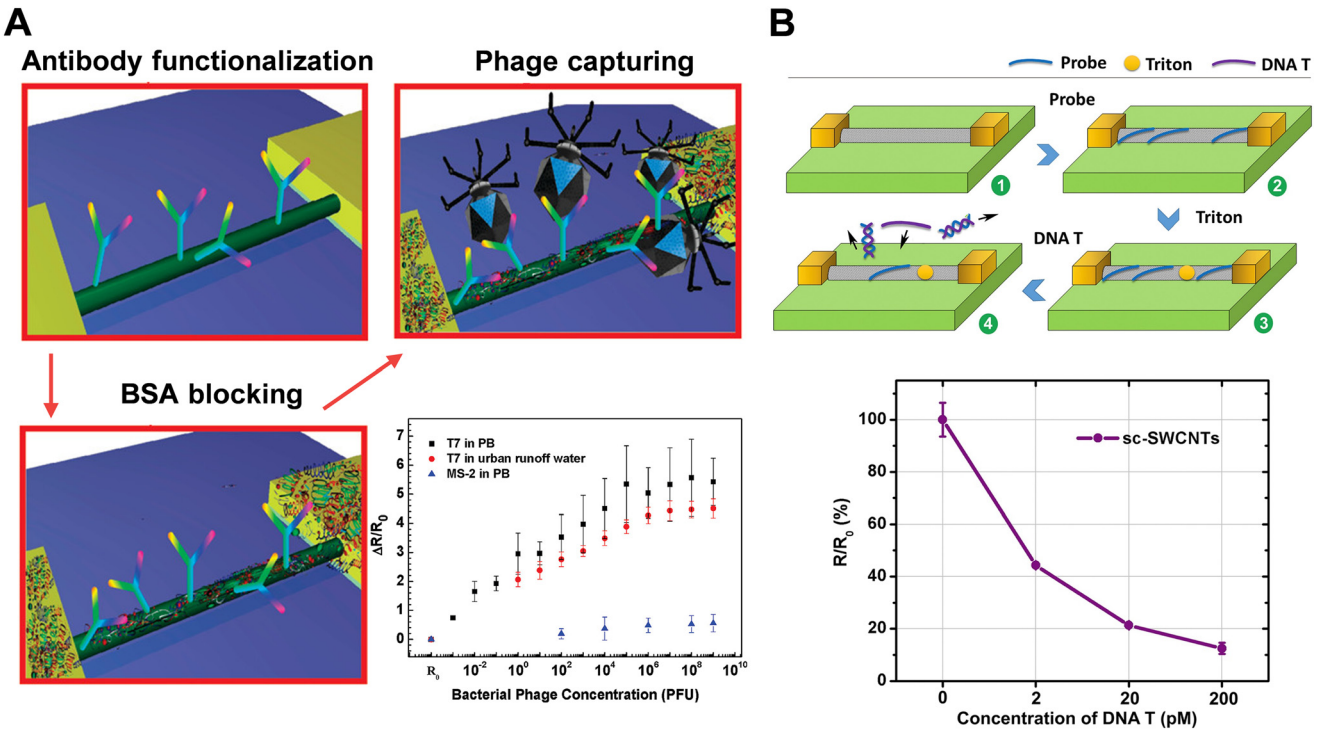

Fig. 7 Chemiresistor detection of viruses. (A) Antibody functionalization, BSA blocking, T7 phage capturing, and sensing responses on the sensor surface. The sensor showed high specificty towards T7 phage. Adapted with permission from ref. 166. Copyright 2010 American Chemical Society. (B) Schematic illustration of CNT-based chemiresistor functionalization and sensing procedures for influenza A virus H5N1 DNA. The increase in DNA concentration caused a decrease in resistant signal. Adapted with permission from ref. 171. Copyright 2017 Elsevier B.V.

functionalized with DNA probe sequences. The DNA probe sequences significantly increase in the relative resistance for CNTs, which provide high initial resistance. When the target complementary DNA sequences were hybridized, a significant decrease in device resistance was observed. The resistance change maintained a continuous downward trend when the concentration ranged from 2 pM to 2 nM.

The resistance of virus-binding chemiresistors can be affected by some other substances (*e.g.*, proteins) as has been reported by Bhasin *et al.*[172] In their work, they found that the high resistance of filamentous M13 virus-binding chemiresistors could be decreased in the presence of human serum albumin (HSA) and could be used for the quantification of HSA in the system. It is a promising work for the detection of protein. Nevertheless, we note that the presence of co-contaminants might significantly affect the viral chemiresistor electrical signal. If such a method was adopted, it would be important to consider the chemical properties of the solution.

3.2.3 Field-effect transistor (FET) based nanosensors. FET-based nanosensors are semiconductor devices with three terminals (*i.e.*, source, drain, and gate)[173] and the electrical carriers flow in the nanoscale semiconductor channel below the gate between the source and drain. When the analytes with charges bind to the gate, the channel's electrical carrier density and current can change due to the electrostatic interaction for biosensing signal transduction. SiNWs, CNTs, and graphene are the most commonly used semiconductor channel nanomaterials due to their high selectivity and sensitivity, real-time response, and label-free detection capabilities.[174,175] For optimal detection sensitivity, it requires careful engineering of semiconductor nanomaterials in device geometry, doping density, and surface properties.[176,177]

Recognition elements are usually necessary for FETs and viruses can be detected by monitoring the change in FET conductivity following viral binding to recognition elements on the channel. Jin *et al.* developed anti-EBOV immobilized reduced graphene oxide (rGO)-FETs to detect inactivated EBOV.[178] A shift in the Dirac voltage was measured when EBOV approached and the LOD reached as low as 2.4 pg mL^{-1}. The rGO-FETs showed negligible conductance changes for other viruses, indicating high target specificity. Similarly, Seo *et al.* recently developed graphene-based FETs for SARS-CoV-2 detection (Fig. 8).[179] The SARS-CoV-2 spike antibody was conjugated onto the graphene sheet *via* 1-pyrenebutyric acid *n*-hydroxysuccinimide ester. Graphene-based FETs successfully detected SARS-CoV-2 at a low level of 16 PFU mL^{-1} in culture medium and showed great potential for clinical samples (242 copies per mL). Fathi-Hafshejani *et al.* reported using a FET sensor for sensitive *in vitro* detection of SARS-CoV-2.[180] The sensor was created by functionalizing tungsten diselenide (WSe_2) monolayers with a monoclonal antibody against SARS-CoV-2 spike protein and exhibited a LOD of ~25 fg μL^{-1} in PBS. Additional applications of antibody immobilized FETs can

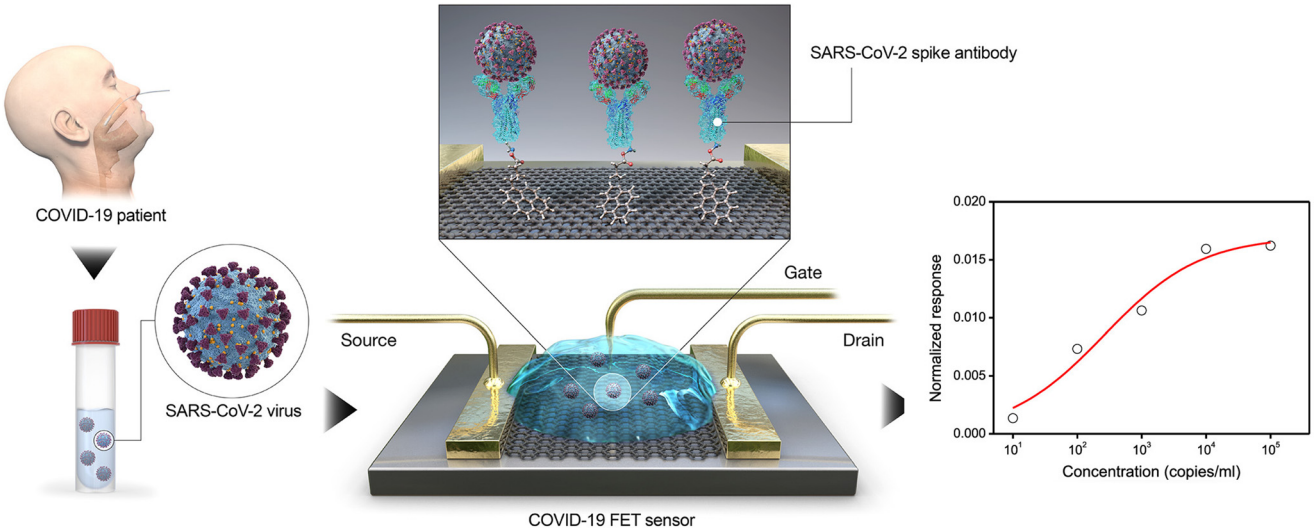

Fig. 8 FET-based nanosensors for SARS-CoV-2 detection through the SARS-CoV-2 spike antibody conjugated graphene sheet. The signal response increase with the concentration of SARS-CoV-2 from clinical samples. Adapted with permission from ref. 179. Copyright 2020 American Chemical Society.

be found elsewhere.[181–183] Using an antibody–antigen reaction, H3N2 in simulated aerosol can be detected within 1–2 min by SiNW-FETs, extending the system to field applications.[182]

In addition to antibodies, other recognition elements have also been used in FETs. Uhm *et al.* developed ultrasensitive SiNW-based FETs for POC detection of H1N1.[184] Cytidine-5′-monophospho-*N*-acetylneuraminic acid (CMP-NANA) was employed as a probe since it can specifically bind both to the aldehyde self-aligned monolayer on the SiNWs and the hemagglutinin 1 domain of hemagglutinin on the surface of H1N1 simultaneously. The threshold voltage shift could reach 112 mV at 1 fM hemagglutinin 1 domain, indicating high sensitivity for H1N1. Recently, Park *et al.* developed a dual-gate FET by functionalizing ACE2 to specifically capture SARS-CoV-2.[185] The developed sensor can successfully detect SARS-CoV-2 in 20 min with a LOD of ~165 copies per mL.

In addition to the direct detection of virus particles, nucleic acids have also been used to determine viruses by FETs. The hybridization of probe DNA and the target DNA/RNA can lead to a change in charge density that induces a change in the electric field. The immobilization of the DNA probe can first affect the output signals. Using CNTs–FETs to detect H1N1 DNA, Tran *et al.* found that if the density of probe DNA was too high, the strongly repulsive electrostatic force among the bases of the DNA strands would make it disadvantageous for the DNA interaction.[186] By optimizing the experimental conditions, the response time of the DNA sensor was less than one minute and the LOD for H1N1 DNA reached 1 pM. Gao *et al.* reported an ultrasensitive poly-L-lysine (PLL)-functionalized graphene FET sensor for breast cancer cell miRNAs and SARS-CoV-2 RNA detection.[187] PLL exhibits a high affinity toward graphene and nucleic acids which can enhance the immobilization of DNA probes. The developed sensor-enabled SARS-CoV-2 RNA detection with a LOD of as low as 1 fM within 20 min. To enhance the immobilization of the DNA probe, some metal oxide NWs have been used in FETs. Shariati developed FETs based on indium tin oxide (ITO) NWs.[188] The intensive conductance and functional modified surface of ITO NWs increased DNA probe immobilization and target DNA hybridization. The LOD for hepatitis B virus (HBV) DNA was 1 pM. Also, the developed ITO NWs device allowed label-free discrimination between the fully matched and mismatched DNAs, offering a unique advantage over other technologies which require labeling and additional tags.

3.3 Magnetic nanosensors

Optical and electrical nanosensors typically use nanomaterials (or modified nanomaterials) as active transducers with high surface sensitivity to convert analyte binding events into optical and electrical readout signals for virus detection. In contrast, magnetic nanosensors typically act as labels, leading to a change in the magnetic signal.[189] The following section is broken into two parts according to the magnetic signal readout device: magnetoresistance and magnetic relaxation switching.

3.3.1 Magnetoresistance (MR) nanosensors. With combined magnetic and electrical properties, MR nanosensors allow the signal transduction process that the electrical resistance can change in response to the binding of magnetic NPs to the sensor surface. Compared with typical optical nanosensors, MR nanosensors exhibit lower background noise and are less affected by environmental factors such as pH and temperature.[190] MR nanosensors can be further classified into anisotropic magnetoresistance

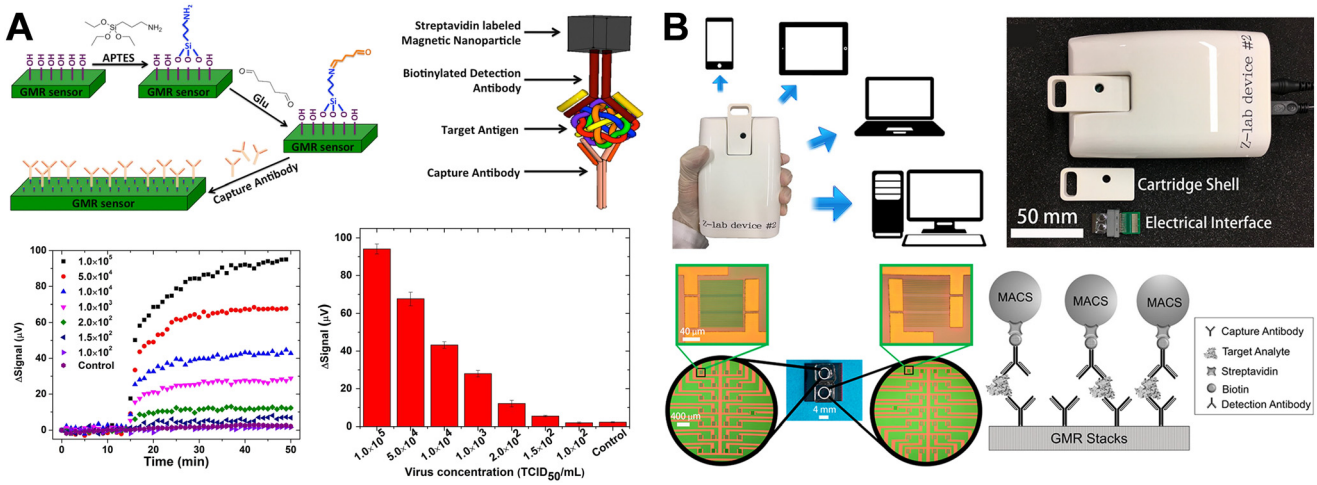

Fig. 9 MR-based nanosensors detection of viruses. (A) Detection of influenza A virus through a typical sandwich structure modified with an antibody. The signal increased with concentration and reaction time. Adapted with permission from ref. 194. Copyright 2016 Frontiers. (B) The portable GMR handheld platform for the detection of the influenza A virus. Adapted with permission from ref. 195. Copyright 2017 American Chemical Society.

(AMR), giant magnetoresistance (GMR), and tunneling magnetoresistance (TMR) nanosensors.[191]

MR nanosensors for virus detection are generally based on the detection of DNA. As discussed by Su *et al.*,[191] most MR nanosensors for detecting DNA can be summarized in the following steps: the DNA probe is first immobilized onto the MR sensor surface. Usually, target DNA is modified with biotin and then attached to the MR sensor surface to hybridize with the DNA probe. Then streptavidin-coated magnetic NPs are added to the MR sensor and captured by the target DNA *via* the strong non-covalent interaction between biotin and streptavidin. Finally, the MR sensor converts the number of adhered magnetic NPs into electrical signals and DNA is quantified. In this way, Yang *et al.* developed MR nanosensors for quick and parallel genotyping of human papilloma virus (HPV) type 16/18.[192] Combined with other technologies, GMR nanosensors can reach low LODs for viruses. For example, Zhi *et al.* successfully detected HBV genotypes by combining GMR nanosensors with LAMP and the LOD is reported to be as low as 10 copies per mL.[193]

Since viral DNA detection requires laborious effort for pretreatment (*e.g.*, DNA extraction), many researchers have turned to directly detecting viral antigen. The mechanism to detect the viral antigen is similar to that for detecting DNA.[191] Capture antibody is modified on the surface of the substrate and binds with the virus and biotinylated detection antibodies in succession. Then, streptavidin-coated magnetic NPs are captured through the biotin–streptavidin reaction. Krishna *et al.* developed a sensitive detection method for

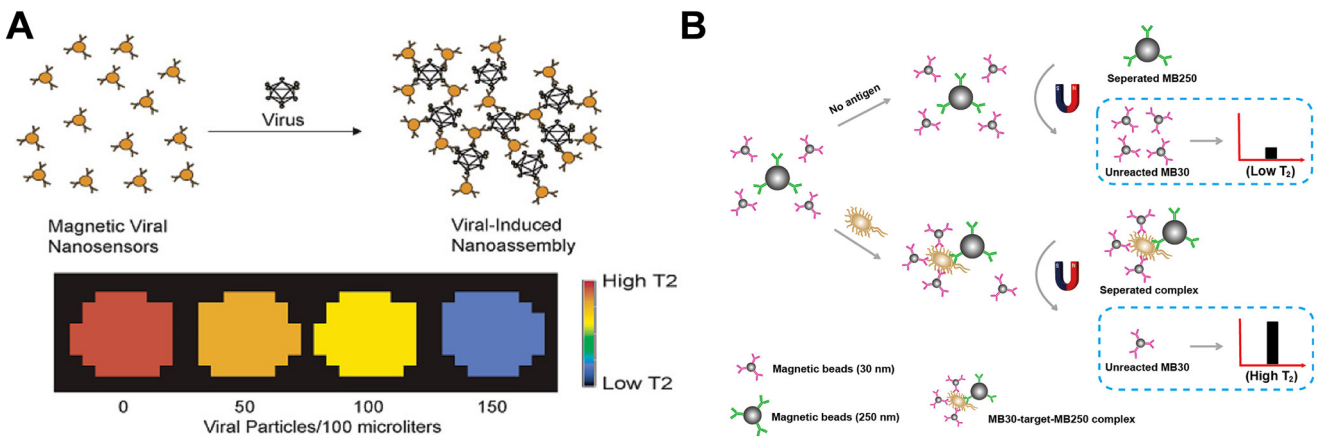

Fig. 10 MRS-based nanosensors detection of viruses. (A) The clustering of the antibody-conjugated magnetic NPs in the presence of the virus occurs with a corresponding change in the MR signal (δT2). Adapted with permission from ref. 199. Copyright 2003 American Chemical Society. (B) The capture and enrichment of the NDV and the T2 signal readout of water molecules around the unreacted MB30. Adapted with permission from ref. 200. Copyright 2015 American Chemical Society.

H1N1 based on GMR nanosensors (Fig. 9A).[194] The capture of magnetic NPs onto the sensors resulted in a resistance change that was measured in real-time by the electrical readout. The sensors could successfully detect H1N1 at levels as low as 150 $TCID_{50}$ mL^{-1}. Subsequently, the same group has worked to improve the detection of viruses by GMR nanosensors. They developed a portable GMR handheld platform for POC H1N1 detection (Fig. 9B).[195] The GMR sensors were embedded in a handheld testing system (Z-Lab) and the real-time change in the magnetoresistance ratio (ΔMR) was monitored for virus quantification. The LOD of this portable Z-lab was 125 $TCID_{50}$ mL^{-1}. Furthermore, they optimized their handheld testing system by adapting the wash-free magnetic bioassay, which was more cost-effective for real-time monitoring and showed great potential for daily sensing.[196]

3.3.2 Magnetic relaxation switching (MRS) nanosensors. MRS nanosensors detect changes in the transverse relaxation time (T2) of the surrounding water molecules caused by the aggregation or disaggregation of magnetic NPs in the presence of an analyte.[197] Generally, such changes can be divided into type I (T2 decreases with the aggregation) or type II (T2 increases with the aggregation). These changes can be monitored by common nucleic magnetic resonance (NMR) and magnetic resonance imaging (MRI) instrumentation.

The behavior of type I and type II based MRS assays for detecting influenza virus hemagglutinin was compared by Koh *et al.*[198] They found that both type I and type II based MRS assays could successfully detect the Tag peptide of influenza virus hemagglutinin using the monoclonal antibody (anti-Tag) modified magnetic NPs. The type II-based assay showed better sensitivity than the type I-based assay. The specificity and sensitivity of the MRS nanosensors can be enhanced by modifying the magnetic NP signal source. Perez *et al.* utilized a bifunctional linker, suberic acid bis (*N*-hydroxysuccinimide ester) to cross-link the amino groups both in the specific antibody and superparamagnetic iron oxide NPs to detect herpes simplex virus (HSV) and AdV in biological media (Fig. 10A).[199] A very low concentration of viral particles (5 viral particles in 10 μL) can cause a detectable magnetic change (δT2) through this method.

To increase the sensitivity of MRS nanosensors and achieve more rapid detection. Chen *et al.* developed a method based on MRS and magnetic separation to detect Newcastle disease virus (NDV) (Fig. 10B).[200] This method takes advantage of the improved magnetic separation of magnetic beads with a larger size (MB_{250}) to capture and enrich target NDV. Smaller magnetic beads (MB_{30}) were chosen as magnetic probes since they could not easily be separated. Following the removal of the MB_{250}–virus–MB_{30} complex, the remaining T2 of MB_{30} was detected and used for quantification of NDV. This approach showed higher sensitivity (10^2 copy per mL) for NDV than the conventional MRS sensor (10^3 copy per mL).

4. Conclusions and future research needs

Understanding virus transmission in the environment and developing rapid and reliable virus detection methods for complicated environmental samples are two pivotal but still unmet needs to address current and future viral outbreaks. Concerted efforts are needed to bridge the disconnect between epidemiological and environmental sciences and enable a proactive and prompt approach to unexpected outbreaks. To date, insufficient knowledge of how viruses spread in many environments makes it difficult to control outbreaks proactively. While highly sensitive, the gold standard PCR-based diagnostics for clinical application suffer from long processing periods and limited supplies.

In this review, we summarized environmental virus transmission routes and then discussed in detail the recent applications of nanosensors for virus detection. Nanosensors can potentially enable rapid response, facile operation, and thus are platforms to advance virus detection more rapidly than conventional approaches. Various nanosensors have been actively developed and show promise for virus detection with high sensitivity, reliability, and a short detection period. Many nanosensors are field-deployable and potentially suitable for mass production. Also, when combined with different analytical tools there is the potential to improve nanosensor efficacy. Micro- or nano-fluidic devices have been successfully incorporated with nanosensors for virus detection.[81,150] Meanwhile, nanosensors can be easily used for POC/POU virus detection through handheld devices.[90,195]

Although the development of nanosensors for virus detection is gradually maturing, there remain issues that need to be addressed if they are to be commercialized for field applications. For instance, while nanosensor sensitivity is readily reported, device and platform stability are much less studied. Virus sampling inevitably comes with interference from environmental, food, and clinical samples that may deteriorate the accuracy of the detection method. Most of the work described in the literature relies upon laboratory settings or is applied to clinical samples. The effects of environmental stressors and interferents (*e.g.*, pH, salinity, organic matter) on detection accuracy must be investigated and reported. Also, despite many developments in nanosensors, most such platforms are currently geared toward medical applications. For successful application of nanosensors in environmental samples, we need environment-centered strategies that improve different aspects of nanosensors (Box 1). Also, future research should be directed to fill the knowledge gaps between related fields such as epidemiology, environmental science and engineering, and aerosol science. We close with a list of standards that reflect the current status of nanosensors for virus detection in the environment and discuss the need for future research (Box 2).

Box 1 Linking virus environmental transmission to nanosensors: potential challenges that need additional research effort

Despite many successes in the development of nanosensors for virus detection, their application in environmental settings remains underexplored relative to clinical samples. The potential impacts of factors from a range of environments should be demonstrated. We condense such strategies into three priorities to realize the application of nanosensors for the detection of viruses in the environment.

1) Environmental transmission

Although we have highlighted environmental routes of viral dissemination, there remains a need for scientific investigation of transmission routes to appropriately design effective sampling strategies. For example, the relative importance of airborne transmission routes of SARS-CoV-2 has been disputed.[201] The appropriate detection approach will be highly dependent upon whether SARS-CoV-2 transmits primarily *via* droplets or aerosols.

2) Environmental media

Environmental composition is dependent upon the specific medium (water, air, food) under consideration. During virus sampling, background constituents will be present along with target viruses and may interfere with nanosensor performance. Accordingly, it is imperative to investigate the potential effects of interferents on the nanosensors. *Water*: suspended solids, natural organic matter (NOM), and inorganic/organic contaminants are common constituents in water samples. pH may also have an impact on nanosensor stability.[13] *Food*: fat and proteins from meat, juice, or milk; cellulose from plant matter; oil and physiological fluids from soils and livestock feces may impact nanosensor performance.[202] *Air*: alkaline species (*e.g.*, ammonia), organic acids (*e.g.*, sulfuric acids) and particulate matter need to be considered. Considering potential inferences from numerous compositions in environmental media, it is important to evaluate the performance of any nanosensor (*e.g.*, LOD) in a range of environments. For example, the real-time RT-PCR and RT-LAMP for detection of SARS-CoV-2 had LODs of 0.41 copies per μL and 0.4 copies per μL in sewage samples.[203,204] Nanosensor sensitivity needs to be evaluated in real environmental media and then the results explicitly compared to conventional approaches under the same conditions.

3) Environmental sampling

The concentration of viruses of interest in environmental samples are often low and thus sampling schemes that are able to concentrate viral loads are an important, yet often poorly considered aspect of effective environmental nanosensor application. Existing approaches for sample concentration include the following. *Water*: samples can be processed by an adsorption–elution method using commercially available filters. *Air*: samples can be collected by a variety of different aerosol samplers. *Food*: samples can be processed using an elution buffer after being cut into small pieces. To date, the recovery rates of such sampling filters and elution buffers have not been explicitly explored nor compared. Establishment of standard methods that report expected recovery rates for different environments remains an important need.

Box 2 Nanosensor criteria for virus detection in environmental samples

Despite the considerable literature on development of nanosensors for virus detection, there remain few reports illustrating their application for environmental sample analysis. Here we summarize the current status of nanosensors for detection of virus in environmental samples and we discuss the need for future research.

Sensitivity and specificity

The sensitivity and specificity of current nanosensors achieved through measurable signal change and specific recognition elements are often reportedly comparable to conventional methods such as RT-PCR and ELISA. (*e.g.*, LODs of nanosensors for SARS-CoV-2 are ~80 copies per mL (ref. 103)). However, complex environmental interferences and the buffers or chemicals involved in the sample handling process may affect nanosensor stability and performance. Sensitivity and specificity should be evaluated using real environmental samples that contain virus, or at a minimum in samples spiked with virus that use representative matrices. Reported LODs and units should be be standardized across the literature for comparison.

Field-deployability and cost

Nanosensors promise device miniaturization and the capacity for multiplex detection with the promised goal of low-cost detection. Considering that samples can be collected from various viral transmission routes at different spatiotemporal scales, the field-deployability and cost of nanosensors are important criteria. Device cost can be reduced through low-cost device fabrication, reductions in sample handling reagents, and through the use of field-deployable read-out device integration. Nanomaterials can be incorporated into paper-based platforms to develop sensor chips or into lateral flow devices.[205] For example, a cotton swab stick-based nanosensor manufactured for 15 cents can be used for the detection of SARS-CoV-2.[206] Low-cost, handheld readout devices such as cell phones and portable Raman instruments are also available and can be operated by solar or battery power.

Turnaround time

Simple and rapid reaction kinetics between the virus and the recognition element of the nanosensor are favorable given the relatively long turnaround times of many conventional methods (*e.g.*, a few hours for PCR-based assays). The output signals following viral recognition can be collected in a short time (*e.g.*, a few seconds[122] to a few minutes,[103] or even in real-time[207]). Such rapid turnaround times can minimize sample manipulation and storage. Data visualization with handheld screens can further help achieve rapid turnaround time.

Abbreviations

Viruses

SARS-CoV	Severe acute respiratory syndrome coronavirus
SARS-CoV-2	Severe acute respiratory syndrome coronavirus 2
MERS-CoV	Middle east respiratory syndrome coronavirus
EBOV	Ebola virus
ZIKV	Zika virus
HAV, HBV, HCV, and HEV	Hepatitis A, B, C and E virus
NoV	Norovirus
AdV	Adenovirus
Ad5	Adenovirus type 5
RV	Rotavirus
CHIKV	Chikungunya virus
DENV	Dengue virus
PCV2	Porcine circovirus type 2
PPV	Porcine parvovirus
PRV	Porcine pseudorabies virus
PVX	Potato virus X
Cv3/CVB3	Coxsackievirus type 3
MYXV	Myxomatosis virus

CDV	Canine distemper virus
CMV	Cucumber mosaic virus
TMV	Tobacco mosaic virus
EMCV	*Encephalomyocarditis* virus
RSV	Respiratory syncytial virus
EV71	Enterovirus 71
CTV	Citrus tristeza virus
ORSV	*Odontoglossum* ringspot virus
ALV	Avian leukosis virus
HPV	Human papilloma virus
HSV	Herpes simplex virus
NDV	Newcastle disease virus

Nanomaterials

NPs	Nanoparticles
NWs	Nanowires
AuNPs and AgNPs	Gold and silver nanoparticles
AuNRs and AgNRs	Gold and silver nanorods
AuNSs	Gold nanostars
AuNZs	Gold nanozymes
Fe_3O_4 NPs	Iron oxide nanoparticles
SiNWs	Silicon nanowires
CNTs	Carbon nanotubes
SWCNTs and MWCNTs	Single-walled and multi-walled carbon nanotubes
AuCNTs	Gold decorated carbon nanotubes
QDs	Quantum dots
RuSi NPs	$Ru(bpy)_3^{2+}$ in silica nanoparticles
CuNCs	Copper nanocomposite
MOFs	Metal–organic frameworks
GO	Graphene oxide
rGO	Reduced graphene oxide
mrGO	Magnetic reduced graphene oxide
V_2O_5	Vanadium oxide
VONP-LPs	V_2O_5-Encapsulated liposomes
TiO_2	Titanium oxide
ZnO	Zinc oxide
ZnONRs	Zinc oxide nanorods
WSe_2	Tungsten diselenide
ITO	Indium tin oxide

Technical terminologies

PCR	Polymerase chain reaction
LAMP	Loop-mediated isothermal amplification
ELISA	Enzyme-linked immunosorbent assays
SELEX	Systematic evolution of ligands by exponential enrichment
RT	Reverse transcription/Reverse transcribed
PFU	Plaque-forming unit
$TCID_{50}$	50% tissue culture infectious dose
HAU	Hemagglutination unit
POC and POU	Point-of-care and point-of-use
LF	Lateral flow
CL	Control line
TL	Test line
LOD	Limit of detection
LDA	Linear discriminant analysis
RH	Relative humidity
SPR	Surface plasmon resonance
LSPR	Localized surface plasmon resonance
SERS	Surface-enhanced Raman scattering
VERS	Volume-enhanced Raman scattering
EM	Electromagnetic
NIR	Near-infrared
DPV	Differential pulse voltammetry
FRET	Fluorescence resonance electron transfer
PAFI	Plasmonic-assisted fluoroimmunoassay
MagLISA	Magnetic nanozyme-linked immunosorbent assay
MFIA	Magnetofluoroimmunoassay
FICT	Fluorescent immunochromatographic strips test
NEA	Nanoelectrode array
SAM	Self-assembled monolayer
FET	Field-effect transistor
EIS	Electrochemical impedance spectroscopy
ECL	Electrochemiluminescence
MR	Magnetoresistance
AMR	Anisotropic magnetoresistance
GMR	Giant magnetoresistance
TMR	Tunneling magnetoresistance
MRS	Magnetic relaxation switching
NMR	Nucleic magnetic resonance
MRI	Magnetic resonance imaging

Chemicals

HRP	Horseradish peroxidase
IgG	Immunoglobulin
TMB	3′,5,5′-Tetramethylbenzidine
H_2O_2	Hydrogen peroxide
PDA	Polydiacetylene
ACE2	Angiotensin-converting enzyme 2
S protein	Spike glycoprotein
GBP	Gold binding peptide
RBITC	Rhodamine B isothiocyanate
MGITC	Malachite green isothiocyanate
OHT	Oseltamivir hexylthiol
Cy3	Cyanine 3
4-ATP	4-Aminothiophenol
6-FAM	6-Carboxyfluorescent
EDC	1-Ethyl-3-(3-dimethylaminopropyl)carbodiimide
NHS	*N*-Hydroxysuccinimide
MB	Methylene blue
Ppy	Polypyrrole
HSA	Human serum albumin
GOD	Glucose oxidase
S RBD	Spike protein receptor binding domain
PLL	Poly-L-lysine
ssDNA	Single-stranded DNA
CMP-NANA	Cytidine-5′-monophospho-*N*-acetylneuraminic acid
PBS	Phosphate-buffered saline

Author contributions

W. Wang and S. Kang directed the research effort, did the literature review, wrote the manuscript, and provided oversight of the research team. W. Zhou aided in the writing of the manuscript. P. J. Vikesland obtained the research funding, provided oversight of the project, and collaborated in the writing and editing of the manuscript. All authors contributed to the development of the manuscript and its revision.

Conflicts of interest

There are no conflicts to declare.

Acknowledgements

This research was supported by the US National Science Foundation grants OISE-1545756 and CBET-2029911. Additional support was provided by the Sustainable Nanotechnology Interdisciplinary Graduate Program (VTSuN IGEP) funded by the Virginia Tech Graduate School. We thank Dr. Linsey C Marr at Virginia Tech for valuable comments on the virus transmission in the environment.

References

1 P. A. Rota, M. S. Oberste, S. S. Monroe, W. A. Nix, R. Campagnoli, J. P. Icenogle, S. Penaranda, B. Bankamp, K. Maher and M.-H. Chen, Characterization of a novel coronavirus associated with severe acute respiratory syndrome, *Science*, 2003, **300**, 1394–1399.

2 D. J. Jamieson, M. A. Honein, S. A. Rasmussen, J. L. Williams, D. L. Swerdlow, M. S. Biggerstaff, S. Lindstrom, J. K. Louie, C. M. Christ and S. R. Bohm, H1N1 2009 influenza virus infection during pregnancy in the USA, *Lancet*, 2009, **374**, 451–458.

3 S. K. Gire, A. Goba, K. G. Andersen, R. S. Sealfon, D. J. Park, L. Kanneh, S. Jalloh, M. Momoh, M. Fullah and G. Dudas, Genomic surveillance elucidates Ebola virus origin and transmission during the 2014 outbreak, *Science*, 2014, **345**, 1369–1372.

4 I. K. Oboho, S. M. Tomczyk, A. M. Al-Asmari, A. A. Banjar, H. Al-Mugti, M. S. Aloraini, K. Z. Alkhaldi, E. L. Almohammadi, B. M. Alraddadi and S. I. Gerber, 2014 MERS-CoV outbreak in Jeddah—a link to health care facilities, *N. Engl. J. Med.*, 2015, **372**, 846–854.

5 G. S. Campos, A. C. Bandeira and S. I. Sardi, Zika virus outbreak, Bahia, Brazil, *Emerging Infect. Dis.*, 2015, **21**, 1885.

6 World Health Organization (WHO), Coronavirus disease 2019 (COVID-19): situation report, Available at: **https://www.who.int/emergencies/diseases/novel-coronavirus-2019/situation-reports**, Accessed June, 2022.

7 I. Kong, Y. Park, Y. Woo, J. Lee, J. Cha, J. Choi, Y. Kim, J. Kim, S. Park and M. Yum, Early epidemiological and clinical characteristics of 28 cases of coronavirus disease in South Korea, *Osong Public Health Res. Perspect.*, 2020, **11**, 8–14.

8 B. Adelodun, F. O. Ajibade, A. O. Tiamiyu, N. A. Nwogwu, R. G. Ibrahim, P. Kumar, V. Kumar, G. Odey, K. K. Yadav and A. H. Khan, Monitoring the presence and persistence of SARS-CoV-2 in water-food-environmental compartments: State of the knowledge and research needs, *Environ. Res.*, 2021, **200**, 111373.

9 World Health Organization (WHO), Modes of transmission of virus causing COVID-19: implications for IPC precaution recommendations: scientific brief, 27 March, 2020.

10 B. Roche and P. Rohani, Environmental transmission scrambles coexistence patterns of avian influenza viruses, *Epidemics*, 2010, **2**, 92–98.

11 R. Gonzalez, K. Curtis, A. Bivins, K. Bibby, M. H. Weir, K. Yetka, H. Thompson, D. Keeling, J. Mitchell and D. Gonzalez, COVID-19 surveillance in Southeastern Virginia using wastewater-based epidemiology, *Water Res.*, 2020, **186**, 116296.

12 P. J. Vikesland and K. R. Wigginton, Nanomaterial Enabled Biosensors for Pathogen Monitoring – A Review, *Environ. Sci. Technol.*, 2010, **44**, 3656–3669.

13 P. J. Vikesland, Nanosensors for water quality monitoring, *Nat. Nanotechnol.*, 2018, **13**, 651–660.

14 D. Rodriguez-Lazaro, N. Cook, F. M. Ruggeri, J. Sellwood, A. Nasser, M. S. J. Nascimento, M. D'Agostino, R. Santos, J. C. Saiz and A. Rzeżutka, Virus hazards from food, water and other contaminated environments, *FEMS Microbiol. Rev.*, 2012, **36**, 786–814.

15 M. Elsamadony, M. Fujii, T. Miura and T. Watanabe, Possible transmission of viruses from contaminated human feces and sewage: Implications for SARS-CoV-2, *Sci. Total Environ.*, 2021, **755**, 142575.

16 B. J. Cowling, D. K. Ip, V. J. Fang, P. Suntarattiwong, S. J. Olsen, J. Levy, T. M. Uyeki, G. M. Leung, J. M. Peiris and T. Chotpitayasunondh, Aerosol transmission is an important mode of influenza A virus spread, *Nat. Commun.*, 2013, **4**, 1935.

17 Z. Altintas, M. Gittens, J. Pocock and I. E. Tothill, Biosensors for waterborne viruses: Detection and removal, *Biochimie*, 2015, **115**, 144–154.

18 I. Xagoraraki, Z. Yin and Z. Svambayev, Fate of viruses in water systems, *J. Environ. Eng.*, 2014, **140**, 04014020.

19 M. V. A. Corpuz, A. Buonerba, G. Vigliotta, T. Zarra, F. Ballesteros Jr, P. Campiglia, V. Belgiorno, G. Korshin and V. Naddeo, Viruses in wastewater: occurrence, abundance and detection methods, *Sci. Total Environ.*, 2020, **745**, 140910.

20 W. Ahmed, B. Tscharke, P. M. Bertsch, K. Bibby, A. Bivins, P. Choi, L. Clarke, J. Dwyer, J. Edson and T. M. H. Nguyen, SARS-CoV-2 RNA monitoring in wastewater as a potential early warning system for COVID-19 transmission in the community: A temporal case study, *Sci. Total Environ.*, 2021, **761**, 144216.

21 S. P. Sherchan, S. Shahin, L. M. Ward, S. Tandukar, T. G. Aw, B. Schmitz, W. Ahmed and M. Kitajima, First detection of SARS-CoV-2 RNA in wastewater in North America: A study in Louisiana, USA, *Sci. Total Environ.*, 2020, **743**, 140621.

22 E. Haramoto, B. Malla, O. Thakali and M. Kitajima, First environmental surveillance for the presence of SARS-CoV-2 RNA in wastewater and river water in Japan, *Sci. Total Environ.*, 2020, **737**, 140405.
23 W. Ahmed, N. Angel, J. Edson, K. Bibby, A. Bivins, J. W. O'Brien, P. M. Choi, M. Kitajima, S. L. Simpson and J. Li, First confirmed detection of SARS-CoV-2 in untreated wastewater in Australia: A proof of concept for the wastewater surveillance of COVID-19 in the community, *Sci. Total Environ.*, 2020, **728**, 138764.
24 C. J. Campos, J. Avant, J. Lowther, D. Till and D. N. Lees, Human norovirus in untreated sewage and effluents from primary, secondary and tertiary treatment processes, *Water Res.*, 2016, **103**, 224–232.
25 X. Pang, Y. Qiu, T. Gao, R. Zurawell, N. F. Neumann, S. Craik and B. E. Lee, Prevalence, levels and seasonal variations of human enteric viruses in six major rivers in Alberta, Canada, *Water Res.*, 2019, **153**, 349–356.
26 H. Lee, M. Kim, J. E. Lee, M. Lim, M. Kim, J. M. Kim, W. H. Jheong, J. Kim and G. Ko, Investigation of norovirus occurrence in groundwater in metropolitan Seoul, Korea, *Sci. Total Environ.*, 2011, **409**, 2078–2084.
27 T. Miura, A. Gima and M. Akiba, Detection of norovirus and rotavirus present in suspended and dissolved forms in drinking water sources, *Food Environ. Virol.*, 2019, **11**, 9–19.
28 H. Wang, I. Kjellberg, P. Sikora, H. Rydberg, M. Lindh, O. Bergstedt and H. Norder, Hepatitis E virus genotype 3 strains and a plethora of other viruses detected in raw and still in tap water, *Water Res.*, 2020, **168**, 115141.
29 C. P. Gerba and W. Q. Betancourt, Assessing the Occurrence of Waterborne Viruses in Reuse Systems: Analytical Limits and Needs, *Pathogens*, 2019, **8**, 107.
30 R. Leiva-Rebollo, A. M. Labella, E. J. Valverde, D. Castro and J. J. Borrego, Persistence of Lymphocystis Disease Virus (LCDV) in Seawater, *Food Environ. Virol.*, 2020, **12**, 174–179.
31 P. Khare and L. Marr, Simulation of vertical concentration gradient of influenza viruses in dust resuspended by walking, *Indoor Air*, 2015, **25**, 428–440.
32 C. C. Wang, K. A. Prather, J. Sznitman, J. L. Jimenez, S. S. Lakdawala, Z. Tufekci and L. C. Marr, Airborne transmission of respiratory viruses, *Science*, 2021, **373**, eabd9149.
33 L. Morawska and J. Cao, Airborne transmission of SARS-CoV-2: The world should face the reality, *Environ. Int.*, 2020, **139**, 105730.
34 M. D. Christian, M. Loutfy, C. McDonald, K. F. Martinez, M. Ofner, T. Wong, T. Wallington, W. L. Gold, B. Mederski, K. Green, D. E. Low and S. I. Team, Possible SARS coronavirus transmission during cardiopulmonary resuscitation, *Emerging Infect. Dis.*, 2004, **10**, 287–293.
35 C. Zemouri, S. Awad, C. Volgenant, W. Crielaard, A. Laheij and J. De Soet, Modeling of the transmission of coronaviruses, measles virus, influenza virus, Mycobacterium tuberculosis, and Legionella pneumophila in dental clinics, *J. Dent. Res.*, 2020, **99**, 1192–1198.
36 X. Zhao, W. Nie, C. Zhou, M. Cheng, C. Wang, Y. Liu, J. Li, Y. Qian, X. Ma and L. Zhang, Airborne Transmission of Influenza Virus in a Hospital of Qinhuangdao During 2017–2018 Flu Season, *Food Environ. Virol.*, 2019, **11**, 427–439.
37 Y. Liu, Z. Ning, Y. Chen, M. Guo, Y. Liu, N. K. Gali, L. Sun, Y. Duan, J. Cai, D. Westerdahl, X. Liu, K. Xu, K.-F. Ho, H. Kan, Q. Fu and K. Lan, Aerodynamic analysis of SARS-CoV-2 in two Wuhan hospitals, *Nature*, 2020, **582**, 557–560.
38 C. Xie, E. H. Lau, T. Yoshida, H. Yu, X. Wang, H. Wu, J. Wei, B. Cowling, M. Peiris and Y. Li, Detection of influenza and other respiratory viruses in air sampled from a university campus: a longitudinal study, *Clin. Infect. Dis.*, 2020, **70**, 850–858.
39 K. K. Coleman and W. V. Sigler, Airborne Influenza A Virus Exposure in an Elementary School, *Sci. Rep.*, 2020, **10**, 1859.
40 K. Lin and L. C. Marr, Humidity-Dependent Decay of Viruses, but Not Bacteria, in Aerosols and Droplets Follows Disinfection Kinetics, *Environ. Sci. Technol.*, 2019, **54**, 1024–1032.
41 J. Tamerius, S. Ojeda, C. K. Uejio, J. Shaman, B. Lopez, N. Sanchez and A. Gordon, Influenza transmission during extreme indoor conditions in a low-resource tropical setting, *Int. J. Biometeorol.*, 2017, **61**, 613–622.
42 P. Wolkoff, Indoor air humidity, air quality, and health–An overview, *Int. J. Hyg. Environ. Health*, 2018, **221**, 376–390.
43 A. Bosch, R. M. Pintó and S. Guix, Foodborne viruses, *Curr. Opin. Food Sci.*, 2016, **8**, 110–119.
44 R. C. Miranda and D. W. Schaffner, Virus risk in the food supply chain, *Curr. Opin. Food Sci.*, 2019, **30**, 43–48.
45 A. Bosch, E. Gkogka, F. S. Le Guyader, F. Loisy-Hamon, A. Lee, L. van Lieshout, B. Marthi, M. Myrmel, A. Sansom, A. C. Schultz, A. Winkler, S. Zuber and T. Phister, Foodborne viruses: Detection, risk assessment, and control options in food processing, *Int. J. Food Microbiol.*, 2018, **285**, 110–128.
46 P. Liu, M. Yang, X. Zhao, Y. Guo, L. Wang, J. Zhang, W. Lei, W. Han, F. Jiang and W. J. Liu, Cold-chain transportation in the frozen food industry may have caused a recurrence of COVID-19 cases in destination: successful isolation of SARS-CoV-2 virus from the imported frozen cod package surface, *Biosaf. Health*, 2020, **2**, 199–201.
47 J. Brassard, M.-J. Gagné, M. Généreux and C. Côté, Detection of human food-borne and zoonotic viruses on irrigated, field-grown strawberries, *Appl. Environ. Microbiol.*, 2012, **78**, 3763–3766.
48 H. Shin, H. Park, D. J. Seo, S. Jung, D. Yeo, Z. Wang, K. H. Park and C. Choi, Foodborne Viruses Detected Sporadically in the Fresh Produce and Its Production Environment in South Korea, *Foodborne Pathog. Dis.*, 2019, **16**, 411–420.
49 Y. Somura, M. Nagano, K. Kimoto, M. Oda, K. Mori, T. Shinkai and K. Sadamasu, Detection of norovirus in food samples collected during suspected food-handler-involved foodborne outbreaks in Tokyo, *Lett. Appl. Microbiol.*, 2019, **69**, 175–180.
50 Y. Lu, M. M. Ma, H. Wang, D. H. Wang, C. Chen, Q. L. Jing, J. M. Geng, T. G. Li, Z. B. Zhang and Z. C. Yang, An

outbreak of norovirus-related acute gastroenteritis associated with delivery food in Guangzhou, southern China, *BMC Public Health*, 2020, **20**, 25.

51 J. Han, X. Zhang, S. He and P. Jia, Can the coronavirus disease be transmitted from food? A review of evidence, risks, policies and knowledge gaps, *Environ. Chem. Lett.*, 2020, **19**, 5–16.

52 K. L. Burkhalter and H. M. Savage, Detection of Zika virus in desiccated mosquitoes by real-time reverse transcription PCR and plaque assay, *Emerging Infect. Dis.*, 2017, **23**, 680–681.

53 S. Pfefferle, S. Reucher, D. Nörz and M. Lütgehetmann, Evaluation of a quantitative RT-PCR assay for the detection of the emerging coronavirus SARS-CoV-2 using a high throughput system, *Eurosurveillance*, 2020, **25**, 2000152.

54 R. Lu, X. Wu, Z. Wan, Y. Li, X. Jin and C. Zhang, A Novel Reverse Transcription Loop-Mediated Isothermal Amplification Method for Rapid Detection of SARS-CoV-2, *Int. J. Mol. Sci.*, 2020, **21**, 2826.

55 F. J. DeGraves, D. Gao and B. Kaltenboeck, High-sensitivity quantitative PCR platform, *BioTechniques*, 2003, **34**, 106–115.

56 C. Uribe-Alvarez, Q. Lam, D. A. Baldwin and J. Chernoff, Low saliva pH can yield false positives results in simple RT-LAMP-based SARS-CoV-2 diagnostic tests, *PLoS One*, 2021, **16**, e0250202.

57 P. Hardinge and J. A. Murray, Reduced false positives and improved reporting of loop-mediated isothermal amplification using quenched fluorescent primers, *Sci. Rep.*, 2019, **9**, 7400.

58 M. N. Aoki, B. de Oliveira Coelho, L. G. B. Góes, P. Minoprio, E. L. Durigon, L. G. Morello, F. K. Marchini, I. N. Riediger, M. do Carmo Debur, H. I. Nakaya and L. Blanes, Colorimetric RT-LAMP SARS-CoV-2 diagnostic sensitivity relies on color interpretation and viral load, *Sci. Rep.*, 2021, **11**, 9026.

59 X. Wang, H. Yao, X. Xu, P. Zhang, M. Zhang, J. Shao, Y. Xiao and H. Wang, Limits of detection of 6 approved RT–PCR kits for the novel SARS-Coronavirus-2 (SARS-CoV-2), *Clin. Chem.*, 2020, **66**, 977–979.

60 Y. He, T. Xie and Y. Tong, Rapid and highly sensitive one-tube colorimetric RT-LAMP assay for visual detection of SARS-CoV-2 RNA, *Biosens. Bioelectron.*, 2021, **187**, 113330.

61 V. Roy, S. Fischinger, C. Atyeo, M. Slein, C. Loos, A. Balazs, C. Luedemann, M. G. Astudillo, D. Yang and D. R. Wesemann, SARS-CoV-2-specific ELISA development, *J. Immunol. Methods*, 2020, **484**, 112832.

62 S. Hosseini, P. Vázquez-Villegas, M. Rito-Palomares and S. O. Martinez-Chapa, in *Enzyme-Linked Immunosorbent Assay (ELISA)*, Springer, 2018, pp. 67–115.

63 D. K. Gramotnev and S. I. Bozhevolnyi, Plasmonics beyond the diffraction limit, *Nat. Photonics*, 2010, **4**, 83–91.

64 J. A. Schuller, E. S. Barnard, W. Cai, Y. C. Jun, J. S. White and M. L. Brongersma, Plasmonics for extreme light concentration and manipulation, *Nat. Mater.*, 2010, **9**, 193–204.

65 L. G. Bousiakou, H. Gebavi, L. Mikac, S. Karapetis and M. Ivanda, Surface Enhanced Raman Spectroscopy for Molecular Identification-a Review on Surface Plasmon Resonance (SPR) and Localised Surface Plasmon Resonance (LSPR) in Optical Nanobiosensing, *Croat. Chem. Acta*, 2019, **92**, 479–494.

66 R. Deng, H. Qu, L. Liang, J. Zhang, B. Zhang, D. Huang, S. Xu, C. Liang and W. Xu, Tracing the therapeutic process of targeted aptamer/drug conjugate on cancer cells by surface-enhanced Raman scattering spectroscopy, *Anal. Chem.*, 2017, **89**, 2844–2851.

67 T.-D. Li, R. Zhang, H. Chen, Z.-P. Huang, X. Ye, H. Wang, A.-M. Deng and J.-L. Kong, An ultrasensitive polydopamine bi-functionalized SERS immunoassay for exosome-based diagnosis and classification of pancreatic cancer, *Chem. Sci.*, 2018, **9**, 5372–5382.

68 J. Chen, Y. Huang, P. Kannan, L. Zhang, Z. Lin, J. Zhang, T. Chen and L. Guo, Flexible and adhesive surface enhance Raman scattering active tape for rapid detection of pesticide residues in fruits and vegetables, *Anal. Chem.*, 2016, **88**, 2149–2155.

69 R. Peng, Y. Si, T. Deng, J. Zheng, J. Li, R. Yang and W. Tan, A novel SERS nanoprobe for the ratiometric imaging of hydrogen peroxide in living cells, *Chem. Commun.*, 2016, **52**, 8553–8556.

70 H. Wei, M. R. Willner, L. C. Marr and P. J. Vikesland, Highly stable SERS pH nanoprobes produced by co-solvent controlled AuNP aggregation, *Analyst*, 2016, **141**, 5159–5169.

71 S. Ghaderi, B. Ramesh and A. M. Seifalian, Fluorescence nanoparticles "quantum dots" as drug delivery system and their toxicity: a review, *J. Drug Targeting*, 2011, **19**, 475–486.

72 U. Resch-Genger, M. Grabolle, S. Cavaliere-Jaricot, R. Nitschke and T. Nann, Quantum dots versus organic dyes as fluorescent labels, *Nat. Methods*, 2008, **5**, 763–775.

73 M. Haase and H. Schäfer, Upconverting nanoparticles, *Angew. Chem., Int. Ed.*, 2011, **50**, 5808–5829.

74 A. Karami, M. Hasani, F. A. Jalilian and R. Ezati, Conventional PCR Assisted Single-Component Assembly of Spherical Nucleic Acids for Simple Colorimetric Detection of SARS-CoV-2, *Sens. Actuators, B*, 2020, **328**, 128971.

75 B. Udugama, P. Kadhiresan, H. N. Kozlowski, A. Malekjahani, M. Osborne, V. Y. Li, H. Chen, S. Mubareka, J. B. Gubbay and W. C. Chan, Diagnosing COVID-19: the disease and tools for detection, *ACS Nano*, 2020, **14**, 3822–3835.

76 S. Talebian, G. G. Wallace, A. Schroeder, F. Stellacci and J. Conde, Nanotechnology-based disinfectants and sensors for SARS-CoV-2, *Nat. Nanotechnol.*, 2020, **15**, 618–621.

77 B. Sepúlveda, P. C. Angelomé, L. M. Lechuga and L. M. Liz-Marzán, LSPR-based nanobiosensors, *Nano Today*, 2009, **4**, 244–251.

78 B. D. Ventura, M. Cennamo, A. Minopoli, R. Campanile, S. B. Censi, D. Terracciano, G. Portella and R. Velotta, Colorimetric test for fast detection of SARS-CoV-2 in nasal and throat swabs, *ACS Sens.*, 2020, **5**, 3043–3048.

79 S. Diegoli, A. L. Manciulea, S. Begum, I. P. Jones, J. R. Lead and J. A. Preece, Interaction between manufactured gold

nanoparticles and naturally occurring organic macromolecules, *Sci. Total Environ.*, 2008, **402**, 51–61.

80 L.-H. Xiong, S. Huang, Y. Huang, F. Yin, F. Yang, Q. Zhang, J. Cheng, R. Zhang and X. He, Ultrasensitive Visualization of Virus via Explosive Catalysis of an Enzyme Muster Triggering Gold Nano-aggregate Disassembly, *ACS Appl. Mater. Interfaces*, 2020, **12**, 12525–12532.

81 N. Saraf, M. Villegas, B. J. Willenberg and S. Seal, Multiplex Viral Detection Platform Based on a Aptamers-Integrated Microfluidic Channel, *ACS Omega*, 2019, **4**, 2234–2240.

82 C. R. Basso, B. P. Crulhas, M. Magro, F. Vianello and V. A. Pedrosa, A new immunoassay of hybrid nanomater conjugated to aptamers for the detection of dengue virus, *Talanta*, 2019, **197**, 482–490.

83 S. Oh, J. Kim, V. T. Tran, D. K. Lee, S. R. Ahmed, J. C. Hong, J. Lee, E. Y. Park and J. Lee, Magnetic nanozyme-linked immunosorbent assay for ultrasensitive influenza A virus detection, *ACS Appl. Mater. Interfaces*, 2018, **10**, 12534–12543.

84 S. R. Ahmed, J. Kim, T. Suzuki, J. Lee and E. Y. Park, Enhanced catalytic activity of gold nanoparticle-carbon nanotube hybrids for influenza virus detection, *Biosens. Bioelectron.*, 2016, **85**, 503–508.

85 S. R. Ahmed, K. Takemeura, T.-C. Li, N. Kitamoto, T. Tanaka, T. Suzuki and E. Y. Park, Size-controlled preparation of peroxidase-like graphene-gold nanoparticle hybrids for the visible detection of norovirus-like particles, *Biosens. Bioelectron.*, 2017, **87**, 558–565.

86 A. B. Ganganboina, A. D. Chowdhury, I. M. Khoris, F. Nasrin, K. Takemura, T. Hara, F. Abe, T. Suzuki and E. Y. Park, Dual modality sensor using liposome-based signal amplification technique for ultrasensitive norovirus detection, *Biosens. Bioelectron.*, 2020, **157**, 112169.

87 S. Song, K. Ha, K. Guk, S.-G. Hwang, J. M. Choi, T. Kang, P. Bae, J. Jung and E.-K. Lim, Colorimetric detection of influenza A (H1N1) virus by a peptide-functionalized polydiacetylene (PEP-PDA) nanosensor, *RSC Adv.*, 2016, **6**, 48566–48570.

88 J.-P. Jeong, E. Cho, D. Yun, T. Kim, I.-S. Lee and S. Jung, Label-free colorimetric detection of influenza antigen based on an antibody-polydiacetylene conjugate and its coated polyvinylidene difluoride membrane, *Polymers*, 2017, **9**, 127.

89 M. Rippa, R. Castagna, S. Brandi, G. Fusco, M. Monini, D. Chen, J. Zhou, J. Zyss and L. Petti, Octupolar Plasmonic Nanosensor Based on Ordered Arrays of Triangular Au Nanopillars for Selective Rotavirus Detection, *ACS Appl. Nano Mater.*, 2020, **3**, 4837–4844.

90 Z. Rong, Q. Wang, N. Sun, X. Jia, K. Wang, R. Xiao and S. Wang, Smartphone-based fluorescent lateral flow immunoassay platform for highly sensitive point-of-care detection of Zika virus nonstructural protein 1, *Anal. Chim. Acta*, 2019, **1055**, 140–147.

91 J. Z. Zhang, *Optical properties and spectroscopy of nanomaterials*, World Scientific, 2009.

92 M. Fleischmann, P. J. Hendra and A. J. McQuillan, Raman spectra of pyridine adsorbed at a silver electrode, *Chem. Phys. Lett.*, 1974, **26**, 163–166.

93 D. L. Jeanmaire and R. P. Van Duyne, Surface Raman spectroelectrochemistry: Part I. Heterocyclic, aromatic, and aliphatic amines adsorbed on the anodized silver electrode, *J. Electroanal. Chem. Interfacial Electrochem.*, 1977, **84**, 1–20.

94 R. A. Halvorson and P. J. Vikesland, Surface-Enhanced Raman Spectroscopy (SERS) for Environmental Analyses, *Environ. Sci. Technol.*, 2010, **44**, 7749–7755.

95 J. Liu and Y. Lu, Preparation of aptamer-linked gold nanoparticle purple aggregates for colorimetric sensing of analytes, *Nat. Protoc.*, 2006, **1**, 246–252.

96 J. Cao, T. Sun and K. T. Grattan, Gold nanorod-based localized surface plasmon resonance biosensors: A review, *Sens. Actuators, B*, 2014, **195**, 332–351.

97 L. E. Kreno, N. G. Greeneltch, O. K. Farha, J. T. Hupp and R. P. Van Duyne, SERS of molecules that do not adsorb on Ag surfaces: a metal–organic framework-based functionalization strategy, *Analyst*, 2014, **139**, 4073–4080.

98 Z. Luo, L. Chen, C. Liang, Q. Wei, Y. Chen and J. Wang, Porous carbon films decorated with silver nanoparticles as a sensitive SERS substrate, and their application to virus identification, *Microchim. Acta*, 2017, **184**, 3505–3511.

99 M. G. Caglayan, E. Kasap, D. Cetin, Z. Suludere and U. Tamer, Fabrication of SERS active gold nanorods using benzalkonium chloride, and their application to an immunoassay for potato virus X, *Microchim. Acta*, 2017, **184**, 1059–1067.

100 X. Zhang, X. Zhang, C. Luo, Z. Liu, Y. Chen, S. Dong, C. Jiang, S. Yang, F. Wang and X. Xiao, Volume-Enhanced Raman Scattering Detection of Viruses, *Small*, 2019, **15**, 1805516.

101 N. N. Durmanov, R. R. Guliev, A. V. Eremenko, I. A. Boginskaya, I. A. Ryzhikov, E. A. Trifonova, E. V. Putlyaev, A. N. Mukhin, S. L. Kalnov and M. V. Balandina, Non-labeled selective virus detection with novel SERS-active porous silver nanofilms fabricated by Electron Beam Physical Vapor Deposition, *Sens. Actuators, B*, 2018, **257**, 37–47.

102 C.-W. Chang, J.-D. Liao, A.-L. Shiau and C.-K. Yao, Non-labeled virus detection using inverted triangular Au nano-cavities arrayed as SERS-active substrate, *Sens. Actuators, B*, 2011, **156**, 471–478.

103 Y. Yang, Y. Peng, C. Lin, L. Long, J. Hu, J. He, H. Zeng, Z. Huang, Z.-Y. Li, M. Tanemura, J. Shi, J. R. Lombardi and X. Luo, Human ACE2-Functionalized Gold "Virus-Trap" Nanostructures for Accurate Capture of SARS-CoV-2 and Single-Virus SERS Detection, *Nano-Micro Lett.*, 2021, **13**, 109.

104 D. Zhang, X. Zhang, R. Ma, S. Deng, X. Wang, X. Wang, X. Zhang, X. Huang, Y. Liu, G. Li, J. Qu, Y. Zhu and J. Li, Ultra-fast and onsite interrogation of Severe Acute Respiratory Syndrome Coronavirus 2 (SARS-CoV-2) in waters via surface enhanced Raman scattering (SERS), *Water Res.*, 2021, **200**, 117243.

105 Z. K. Farka, T. S. Juřík, D. Kovář, L. E. Trnková and P. Skládal, Nanoparticle-based immunochemical biosensors

and assays: recent advances and challenges, *Chem. Rev.*, 2017, **117**, 9973–10042.

106 J. Moon, S. Y. Yi, A. Hwang, G. Eom, J. Sim, J. Jeong, E.-K. Lim, B. H. Chung, B. Kim, J. Jung and T. Kang, Facile and sensitive detection of influenza viruses using SERS antibody probes, *RSC Adv.*, 2016, **6**, 84415–84419.

107 K. Karn-Orachai, K. Sakamoto, R. Laocharoensuk, S. Bamrungsap, S. Songsivilai, T. Dharakul and K. Miki, Extrinsic surface-enhanced Raman scattering detection of influenza A virus enhanced by two-dimensional gold@silver core–shell nanoparticle arrays, *RSC Adv.*, 2016, **6**, 97791–97799.

108 G. Eom, A. Hwang, D. K. Lee, K. Guk, J. Moon, J. Jeong, J. Jung, B. Kim, E.-K. Lim and T. Kang, Superb Specific, Ultrasensitive, and Rapid Identification of the Oseltamivir-Resistant H1N1 Virus: Naked-Eye and SERS Dual-Mode Assay Using Functional Gold Nanoparticles, *ACS Appl. Bio Mater.*, 2019, **2**, 1233–1240.

109 S. G. Hwang, K. Ha, K. Guk, D. K. Lee, G. Eom, S. Song, T. Kang, H. Park, J. Jung and E.-K. Lim, Rapid and simple detection of Tamiflu-resistant influenza virus: Development of oseltamivir derivative-based lateral flow biosensor for point-of-care (POC) diagnostics, *Sci. Rep.*, 2018, **8**, 12999.

110 G. Eom, A. Hwang, H. Kim, S. Yang, D. K. Lee, S. Song, K. Ha, J. Jeong, J. Jung, E.-K. Lim and T. Kang, Diagnosis of Tamiflu-Resistant Influenza Virus in Human Nasal Fluid and Saliva Using Surface-Enhanced Raman Scattering, *ACS Sens.*, 2019, **4**, 2282–2287.

111 H. Chen, S.-G. Park, N. Choi, H.-J. Kwon, T. Kang, M.-K. Lee and J. Choo, Sensitive Detection of SARS-CoV-2 Using a SERS-Based Aptasensor, *ACS Sens.*, 2021, **6**, 2378–2385.

112 I. Shiratori, J. Akitomi, D. A. Boltz, K. Horii, M. Furuichi and I. Waga, Selection of DNA aptamers that bind to influenza A viruses with high affinity and broad subtype specificity, *Biochem. Biophys. Res. Commun.*, 2014, **443**, 37–41.

113 V. I. Kukushkin, N. M. Ivanov, A. A. Novoseltseva, A. S. Gambaryan, I. V. Yaminsky, A. M. Kopylov and E. G. Zavyalova, Highly sensitive detection of influenza virus with SERS aptasensor, *PLoS One*, 2019, **14**, e0216247.

114 X. Fu, Z. Cheng, J. Yu, P. Choo, L. Chen and J. Choo, A SERS-based lateral flow assay biosensor for highly sensitive detection of HIV-1 DNA, *Biosens. Bioelectron.*, 2016, **78**, 530–537.

115 M. Xiao, K. Xie, X. Dong, L. Wang, C. Huang, F. Xu, W. Xiao, M. Jin, B. Huang and Y. Tang, Ultrasensitive detection of avian influenza A (H7N9) virus using surface-enhanced Raman scattering-based lateral flow immunoassay strips, *Anal. Chim. Acta*, 2019, **1053**, 139–147.

116 H. Shen, K. Xie, L. Huang, L. Wang, J. Ye, M. Xiao, L. Ma, A. Jia and Y. Tang, A novel SERS-based lateral flow assay for differential diagnosis of wild-type pseudorabies virus and gE-deleted vaccine, *Sens. Actuators, B*, 2019, **282**, 152–157.

117 C. Wang, C. Wang, X. Wang, K. Wang, Y. Zhu, Z. Rong, W. Wang, R. Xiao and S. Wang, Magnetic SERS strip for sensitive and simultaneous detection of respiratory viruses, *ACS Appl. Mater. Interfaces*, 2019, **11**, 19495–19505.

118 L. Zhan, S. J. Zhen, X. Y. Wan, P. F. Gao and C. Z. Huang, A sensitive surface-enhanced Raman scattering enzyme-catalyzed immunoassay of respiratory syncytial virus, *Talanta*, 2016, **148**, 308–312.

119 D. Paria, K. S. Kwok, P. Raj, P. Zheng, D. H. Gracias and I. Barman, Label-free spectroscopic SARS-CoV-2 detection on versatile nanoimprinted substrates, *Nano Lett.*, 2022, **22**, 3620–3627.

120 J. P. Broughton, X. Deng, G. Yu, C. L. Fasching, V. Servellita, J. Singh, X. Miao, J. A. Streithorst, A. Granados, A. Sotomayor-Gonzalez, K. Zorn, A. Gopez, E. Hsu, W. Gu, S. Miller, C.-Y. Pan, H. Guevara, D. A. Wadford, J. S. Chen and C. Y. Chiu, CRISPR–Cas12-based detection of SARS-CoV-2, *Nat. Biotechnol.*, 2020, **38**, 870–874.

121 X. Weng and S. Neethirajan, Aptamer-based fluorometric determination of norovirus using a paper-based microfluidic device, *Microchim. Acta*, 2017, **184**, 4545–4552.

122 R. L. Pinals, F. Ledesma, D. Yang, N. Navarro, S. Jeong, J. E. Pak, L. Kuo, Y.-C. Chuang, Y.-W. Cheng, H.-Y. Sun and M. P. Landry, Rapid SARS-CoV-2 spike protein detection by carbon nanotube-based near-infrared nanosensors, *Nano Lett.*, 2021, **21**, 2272–2280.

123 Y. Cao, T. Xie, R. C. Qian and Y. T. Long, Plasmon resonance energy transfer: coupling between chromophore molecules and metallic nanoparticles, *Small*, 2017, **13**, 1601955.

124 T. R. Shojaei, M. A. M. Salleh, K. Sijam, R. A. Rahim, A. Mohsenifar, R. Safarnejad and M. Tabatabaei, Detection of Citrus tristeza virus by using fluorescence resonance energy transfer-based biosensor, *Spectrochim. Acta, Part A*, 2016, **169**, 216–222.

125 K. Takemura, O. Adegoke, N. Takahashi, T. Kato, T.-C. Li, N. Kitamoto, T. Tanaka, T. Suzuki and E. Y. Park, Versatility of a localized surface plasmon resonance-based gold nanoparticle-alloyed quantum dot nanobiosensor for immunofluorescence detection of viruses, *Biosens. Bioelectron.*, 2017, **89**, 998–1005.

126 J. Lee, S. R. Ahmed, S. Oh, J. Kim, T. Suzuki, K. Parmar, S. S. Park, J. Lee and E. Y. Park, A plasmon-assisted fluoro-immunoassay using gold nanoparticle-decorated carbon nanotubes for monitoring the influenza virus, *Biosens. Bioelectron.*, 2015, **64**, 311–317.

127 S. Link and M. A. El-Sayed, Size and temperature dependence of the plasmon absorption of colloidal gold nanoparticles, *J. Phys. Chem. B*, 1999, **103**, 4212–4217.

128 F. Nasrin, A. D. Chowdhury, K. Takemura, I. Kozaki, H. Honda, O. Adegoke and E. Y. Park, Fluorometric virus detection platform using quantum dots-gold nanocomposites optimizing the linker length variation, *Anal. Chim. Acta*, 2020, **1109**, 148–157.

129 J.-J. Wang, Y.-Z. Jiang, Y. Lin, L. Wen, C. Lv, Z.-L. Zhang, G. Chen and D.-W. Pang, Simultaneous point-of-care detection of enterovirus 71 and coxsackievirus B3, *Anal. Chem.*, 2015, **87**, 11105–11112.

130 K. Takemura, J. Lee, T. Suzuki, T. Hara, F. Abe and E. Y. Park, Ultrasensitive detection of norovirus using a

magnetofluoroimmunoassay based on synergic properties of gold/magnetic nanoparticle hybrid nanocomposites and quantum dots, *Sens. Actuators, B*, 2019, **296**, 126672.

131 S.-T. Yu, C. T. Bui, D. T. H. Kim, A. V. Nguyen, T. T. T. Trinh and S.-J. Yeo, Clinical evaluation of rapid fluorescent diagnostic immunochromatographic test for influenza A virus (H1N1), *Sci. Rep.*, 2018, **8**, 13468.

132 A. V. T. Nguyen, T. D. Dao, T. T. T. Trinh, D.-Y. Choi, S.-T. Yu, H. Park and S.-J. Yeo, Sensitive detection of influenza a virus based on a CdSe/CdS/ZnS quantum dot-linked rapid fluorescent immunochromatographic test, *Biosens. Bioelectron.*, 2020, **155**, 112090.

133 S.-J. Yeo, D. T. Bao, G.-E. Seo, C. T. Bui, D. T. H. Kim, N. T. V. Anh, T. T. T. Tien, N. T. P. Linh, H.-J. Sohn, C.-K. Chong, H.-J. Shin and H. Park, Improvement of a rapid diagnostic application of monoclonal antibodies against avian influenza H7 subtype virus using Europium nanoparticles, *Sci. Rep.*, 2017, **7**, 7933.

134 L. Xu, R. Wang, L. C. Kelso, Y. Ying and Y. Li, A target-responsive and size-dependent hydrogel aptasensor embedded with QD fluorescent reporters for rapid detection of avian influenza virus H5N1, *Sens. Actuators, B*, 2016, **234**, 98–108.

135 X. Kou, S. Jiang, S.-J. Park and L.-Y. Meng, A review: recent advances in preparations and applications of heteroatom-doped carbon quantum dots, *Dalton Trans.*, 2020, **49**, 6915–6938.

136 Z. Huang, G. Zhai, Z. Zhang, C. Zhang, Y. Xia, L. Lian, X. Fu, D. Zhang and J. Zhang, Low cost and large scale synthesis of PbS quantum dots with hybrid surface passivation, *CrystEngComm*, 2017, **19**, 946–951.

137 S. Shen, J. Wang, Z. Wu, Z. Du, Z. Tang and J. Yang, Graphene quantum dots with high yield and high quality synthesized from low cost precursor of aphanitic graphite, *Nanomaterials*, 2020, **10**, 375.

138 Y. Chen, S. Li, L. Huang and D. Pan, Low-cost and gram-scale synthesis of water-soluble Cu–In–S/ZnS core/shell quantum dots in an electric pressure cooker, *Nanoscale*, 2014, **6**, 1295–1298.

139 Z. Meng, R. M. Stolz, L. Mendecki and K. A. Mirica, Electrically-transduced chemical sensors based on two-dimensional nanomaterials, *Chem. Rev.*, 2019, **119**, 478–598.

140 K. Khalid, X. F. Tan, H. F. M. Zaid, Y. Tao, C. L. Chew, D. T. Chu, M. K. Lam, Y. C. Ho, J. W. Lim and L. C. Wei, Advanced in developmental organic and inorganic nanomaterial: a review, *Bioengineered*, 2020, **11**, 328–355.

141 G. T. Chandran, X. W. Li, A. Ogata and R. M. Penner, Electrically Transduced Sensors Based on Nanomaterials (2012-2016), *Anal. Chem.*, 2017, **89**, 249–275.

142 T. Ozer, B. J. Geiss and C. S. Henry, Chemical and biological sensors for viral detection, *J. Electrochem. Soc.*, 2019, **167**, 037523.

143 F. R. Baptista, S. A. Belhout, S. Giordani and S. J. Quinn, Recent developments in carbon nanomaterial sensors, *Chem. Soc. Rev.*, 2015, **44**, 4433–4453.

144 J. M. George, A. Antony and B. Mathew, Metal oxide nanoparticles in electrochemical sensing and biosensing: a review, *Microchim. Acta*, 2018, **185**, 358.

145 F. R. Madiyar, S. L. Haller, O. Farooq, S. Rothenburg, C. Culbertson and J. Li, Ac dielectrophoretic manipulation and electroporation of vaccinia virus using carbon nanoelectrode arrays, *Electrophoresis*, 2017, **38**, 1515–1525.

146 L. Sepunaru, B. J. Plowman, S. V. Sokolov, N. P. Young and R. G. Compton, Rapid electrochemical detection of single influenza viruses tagged with silver nanoparticles, *Chem. Sci.*, 2016, **7**, 3892–3899.

147 B. Piro and S. Reisberg, Recent Advances in Electrochemical Immunosensors, *Sensors*, 2017, **17**, 794.

148 W.-J. Wang, C.-H. Lee, C.-W. Li, S. Liao, F.-J. Jan and G.-J. Wang, Orchid Virus Detection from Orchid Leaves Using Micro/Nano Hybrid-Structured Immuno-Electrochemical Biosensor, *J. Electrochem. Soc.*, 2020, **167**, 027530.

149 A. Sharma, A. Kaushal and S. Kulshrestha, A Nano-Au/C-MWCNT based label free amperometric immunosensor for the detection of capsicum chlorosis virus in bell pepper, *Arch. Virol.*, 2017, **162**, 2047–2052.

150 J.-H. Han, D. Lee, C. H. C. Chew, T. Kim and J. J. Pak, A multi-virus detectable microfluidic electrochemical immunosensor for simultaneous detection of H1N1, H5N1, and H7N9 virus using ZnO nanorods for sensitivity enhancement, *Sens. Actuators, B*, 2016, **228**, 36–42.

151 S. A. Hashemi, N. G. G. Behbahan, S. Bahrani, S. M. Mousavi, A. Gholami, S. Ramakrishna, M. Firoozsani, M. Moghadami, K. B. Lankarani and N. Omidifar, Ultra-sensitive viral glycoprotein detection NanoSystem toward accurate tracing SARS-CoV-2 in biological/non-biological media, *Biosens. Bioelectron.*, 2021, **171**, 112731.

152 H. Zhao, W. Xie, R.-L. Zhang, X.-D. Wang, H.-F. Liu, J. Li, T. Sha, X.-S. Guo, Q.-M. Sun and Y.-P. Zhang, Electrochemical sensor for human norovirus based on covalent organic framework/pillararene heterosupramolecular nanocomposites, *Talanta*, 2022, **237**, 122896.

153 S. H. Baek, C. Y. Park, T. P. Nguyen, M. W. Kim, J. P. Park, C. Choi, S. Y. Kim, S. K. Kailasa and T. J. Park, Novel peptides functionalized gold nanoparticles decorated tungsten disulfide nanoflowers as the electrochemical sensing platforms for the norovirus in an oyster, *Food Control*, 2020, **114**, 107225.

154 M. Backer, C. Koch, S. Eiben, F. Geiger, F. Eber, H. Gliemann, A. Poghossian, C. Wege and M. J. Schoning, Tobacco mosaic virus as enzyme nanocarrier for electrochemical biosensors, *Sens. Actuators, B*, 2017, **238**, 716–722.

155 H. Ilkhani and S. Farhad, A novel electrochemical DNA biosensor for Ebola virus detection, *Anal. Biochem.*, 2018, **557**, 151–155.

156 K. Shang, X. D. Wang, B. Sun, Z. G. Cheng and S. Y. Ai, beta-cyclodextrin-ferrocene host-guest complex multifunctional labeling triple amplification strategy for electrochemical immunoassay of subgroup J of avian leukosis viruses, *Biosens. Bioelectron.*, 2013, **45**, 40–45.

157 F. Luo, C. Long, Z. Wu, H. Xiong, M. Chen, X. Zhang, W. Wen and S. Wang, Functional silica nanospheres for sensitive detection of H9N2 avian influenza virus based on immunomagnetic separation, *Sens. Actuators, B*, 2020, **310**, 127831.

158 J. Li, Y. Li, X. Zhai, Y. Cao, J. Zhao, Y. Tang and K. Han, Sensitive electrochemical detection of hepatitis C virus subtype based on nucleotides assisted magnetic reduced graphene oxide-copper nano-composite, *Electrochem. Commun.*, 2020, **110**, 106601.

159 C. Singhal, C. Pundir and J. Narang, A genosensor for detection of consensus DNA sequence of Dengue virus using ZnO/Pt-Pd nanocomposites, *Biosens. Bioelectron.*, 2017, **97**, 75–82.

160 M. A. Tahir, S. Z. Bajwa, S. Mansoor, R. W. Briddon, W. S. Khan, B. E. Scheffler and I. Amin, Evaluation of carbon nanotube based copper nanoparticle composite for the efficient detection of agroviruses, *J. Hazard. Mater.*, 2018, **346**, 27–35.

161 M. Alafeef, K. Dighe, P. Moitra and D. Pan, Rapid, Ultrasensitive, and Quantitative Detection of SARS-CoV-2 Using Antisense Oligonucleotides Directed Electrochemical Biosensor Chip, *ACS Nano*, 2020, **14**, 17028–17045.

162 H. Zhao, F. Liu, W. Xie, T.-C. Zhou, J. OuYang, L. Jin, H. Li, C.-Y. Zhao, L. Zhang and J. Wei, Ultrasensitive supersandwich-type electrochemical sensor for SARS-CoV-2 from the infected COVID-19 patients using a smartphone, *Sens. Actuators, B*, 2021, **327**, 128899.

163 T. Chaibun, J. Puenpa, T. Ngamdee, N. Boonapatcharoen, P. Athamanolap, A. P. O'Mullane, S. Vongpunsawad, Y. Poovorawan, S. Y. Lee and B. Lertanantawong, Rapid electrochemical detection of coronavirus SARS-CoV-2, *Nat. Commun.*, 2021, **12**, 802.

164 A. Kaushik, A. Yndart, S. Kumar, R. D. Jayant, A. Vashist, A. N. Brown, C.-Z. Li and M. Nair, A sensitive electrochemical immunosensor for label-free detection of Zika-virus protein, *Sci. Rep.*, 2018, **8**, 9700.

165 M. Z. M. Nasir, J. A. Jackman, N.-J. Cho, A. Ambrosi and M. Pumera, Detection of amphipathic viral peptide on screen-printed electrodes by liposome rupture impact voltammetry, *Anal. Chem.*, 2017, **89**, 11753–11757.

166 D. J. Shirale, M. A. Bangar, M. Park, M. V. Yates, W. Chen, N. V. Myung and A. Mulchandani, Label-free chemiresistive immunosensors for viruses, *Environ. Sci. Technol.*, 2010, **44**, 9030–9035.

167 N. Chartuprayoon, Y. Rheem, J. C. K. Ng, J. Nam, W. Chen and N. V. Myung, Polypyrrole nanoribbon based chemiresistive immunosensors for viral plant pathogen detection, *Anal. Methods*, 2013, **5**, 3497–3502.

168 J. Vlasak and R. Ionescu, Fragmentation of monoclonal antibodies, *mAbs*, 2011, **3**, 253–263.

169 D. Wasik, A. Mulchandani and M. V. Yates, A heparin-functionalized carbon nanotube-based affinity biosensor for dengue virus, *Biosens. Bioelectron.*, 2017, **91**, 811–816.

170 N. Varghese, U. Mogera, A. Govindaraj, A. Das, P. K. Maiti, A. K. Sood and C. Rao, Binding of DNA nucleobases and nucleosides with graphene, *ChemPhysChem*, 2009, **10**, 206–210.

171 Y. Fu, V. Romay, Y. Liu, B. Ibarlucea, L. Baraban, V. Khavrus, S. Oswald, A. Bachmatiuk, I. Ibrahim and M. Rümmeli, Chemiresistive biosensors based on carbon nanotubes for label-free detection of DNA sequences derived from avian influenza virus H5N1, *Sens. Actuators, B*, 2017, **249**, 691–699.

172 A. Bhasin, A. F. Ogata, J. S. Briggs, P. Y. Tam, M. X. Tan, G. A. Weiss and R. M. Penner, The Virus Bioresistor: Wiring Virus Particles for the Direct, Label-Free Detection of Target Proteins, *Nano Lett.*, 2018, **18**, 3623–3629.

173 K. I. Chen, B. R. Li and Y. T. Chen, Silicon nanowire field-effect transistor-based biosensors for biomedical diagnosis and cellular recording investigation, *Nano Today*, 2011, **6**, 131–154.

174 M. O. Noor and U. J. Krull, Silicon nanowires as field-effect transducers for biosensor development: A review, *Anal. Chim. Acta*, 2014, **825**, 1–25.

175 V. Schroeder, S. Savagatrup, M. He, S. B. Ling and T. M. Swager, Carbon Nanotube Chemical Sensors, *Chem. Rev.*, 2019, **119**, 599–663.

176 J. S. Li, Y. L. Zhang, S. To, L. D. You and Y. Sun, Effect of Nanowire Number, Diameter, and Doping Density on Nano-FET Biosensor Sensitivity, *ACS Nano*, 2011, **5**, 6661–6668.

177 W. Zhou, X. Dai and C. M. Lieber, Advances in nanowire bioelectronics, *Rep. Prog. Phys.*, 2016, **80**, 016701.

178 X. Jin, H. Zhang, Y. T. Li, M. M. Xiao, Z. L. Zhang, D. W. Pang, G. Wong, Z. Y. Zhang and G. J. Zhang, A field effect transistor modified with reduced graphene oxide for immunodetection of Ebola virus, *Microchim. Acta*, 2019, **186**, 223.

179 G. Seo, G. Lee, M. J. Kim, S.-H. Baek, M. Choi, K. B. Ku, C.-S. Lee, S. Jun, D. Park and H. G. Kim, Rapid Detection of COVID-19 Causative Virus (SARS-CoV-2) in Human Nasopharyngeal Swab Specimens Using Field-Effect Transistor-Based Biosensor, *ACS Nano*, 2020, **14**, 5135–5142.

180 P. Fathi-Hafshejani, N. Azam, L. Wang, M. A. Kuroda, M. C. Hamilton, S. Hasim and M. Mahjouri-Samani, Two-dimensional-material-based field-effect transistor biosensor for detecting COVID-19 virus (SARS-CoV-2), *ACS Nano*, 2021, **15**, 11461–11469.

181 Y. T. Chen, R. Ren, H. H. Pu, X. R. Guo, J. B. Chang, G. H. Zhou, S. Mao, M. Kron and J. H. Chen, Field-Effect Transistor Biosensor for Rapid Detection of Ebola Antigen, *Sci. Rep.*, 2017, **7**, 10974.

182 F. X. Shen, M. M. Tan, Z. X. Wang, M. S. Yao, Z. Q. Xu, Y. Wu, J. D. Wang, X. F. Guo and T. Zhu, Integrating Silicon Nanowire Field Effect Transistor, Microfluidics and Air Sampling Techniques For Real-Time Monitoring Biological Aerosols, *Environ. Sci. Technol.*, 2011, **45**, 7473–7480.

183 A. Maity, X. Sui, B. Jin, H. Pu, K. J. Bottum, X. Huang, J. Chang, G. Zhou, G. Lu and J. Chen, Resonance-Frequency Modulation for Rapid, Point-of-Care Ebola-Glycoprotein Diagnosis with a Graphene-Based Field-Effect Biotransistor, *Anal. Chem.*, 2018, **90**, 14230–14238.

184 M. Uhm, J. M. Lee, J. Lee, J. H. Lee, S. Choi, B. G. Park, D. M. Kim, S. J. Choi, H. S. Mo, Y. J. Jeong and D. H. Kim, Ultrasensitive Electrical Detection of Hemagglutinin for Point-of-Care Detection of Influenza Virus Based on a CMP-NANA Probe and Top-Down Processed Silicon Nanowire Field-Effect Transistors, *Sensors*, 2019, **19**, 4502.

185 S. Park, H. Kim, K. Woo, J.-M. Kim, H.-J. Jo, Y. Jeong and K. H. Lee, SARS-CoV-2 Variant Screening Using a Virus-Receptor-Based Electrical Biosensor, *Nano Lett.*, 2021, **22**, 50–57.

186 T. L. Tran, T. T. Nguyen, T. T. H. Tran, Q. T. Tran and A. T. Mai, Detection of influenza A virus using carbon nanotubes field effect transistor based DNA sensor, *Phys. E*, 2017, **93**, 83–86.

187 J. Gao, C. Wang, C. Wang, Y. Chu, S. Wang, M. Y. Sun, H. Ji, Y. Gao, Y. Wang and Y. Han, Poly-l-Lysine-Modified Graphene Field-Effect Transistor Biosensors for Ultrasensitive Breast Cancer miRNAs and SARS-CoV-2 RNA Detection, *Anal. Chem.*, 2022, **94**, 1626–1636.

188 M. Shariati, The field effect transistor DNA biosensor based on ITO nanowires in label-free hepatitis B virus detecting compatible with CMOS technology, *Biosens. Bioelectron.*, 2018, **105**, 58–64.

189 C. R. Tamanaha, S. P. Mulvaney, J. C. Rife and L. J. Whitman, Magnetic labeling, detection, and system integration, *Biosens. Bioelectron.*, 2008, **24**, 1–13.

190 B. Srinivasan, Y. Li, Y. Jing, Y. Xu, X. Yao, C. Xing and J. P. Wang, A detection system based on giant magnetoresistive sensors and high-moment magnetic nanoparticles demonstrates zeptomole sensitivity: Potential for personalized medicine, *Angew. Chem., Int. Ed.*, 2009, **48**, 2764–2767.

191 D. Su, K. Wu, R. Saha, C. Peng and J.-P. Wang, Advances in Magnetoresistive Biosensors, *Micromachines*, 2020, **11**, 34.

192 H. Yang, L. Chen, C. Lei, J. Zhang, D. Li, Z.-M. Zhou, C.-C. Bao, H.-Y. Hu, X. Chen and F. Cui, Giant magnetoimpedance-based microchannel system for quick and parallel genotyping of human papilloma virus type 16/18, *Appl. Phys. Lett.*, 2010, **97**, 043702.

193 X. Zhi, M. Deng, H. Yang, G. Gao, K. Wang, H. Fu, Y. Zhang, D. Chen and D. Cui, A novel HBV genotypes detecting system combined with microfluidic chip, loop-mediated isothermal amplification and GMR sensors, *Biosens. Bioelectron.*, 2014, **54**, 372–377.

194 V. D. Krishna, K. Wu, A. M. Perez and J.-P. Wang, Giant magnetoresistance-based biosensor for detection of influenza A virus, *Front. Microbiol.*, 2016, **7**, 400.

195 K. Wu, T. Klein, V. D. Krishna, D. Su, A. M. Perez and J.-P. Wang, Portable GMR handheld platform for the detection of influenza A virus, *ACS Sens.*, 2017, **2**, 1594–1601.

196 D. Su, K. Wu, V. Krishna, T. Klein, J. Liu, Y. Feng, A. M. Perez, M. C. Cheeran and J.-P. Wang, Detection of influenza a virus in swine nasal swab samples with a wash-free magnetic bioassay and a handheld giant magnetoresistance sensing system, *Front. Microbiol.*, 2019, **10**, 1077.

197 L. H. Reddy, J. L. Arias, J. Nicolas and P. Couvreur, Magnetic nanoparticles: design and characterization, toxicity and biocompatibility, pharmaceutical and biomedical applications, *Chem. Rev.*, 2012, **112**, 5818–5878.

198 I. Koh, R. Hong, R. Weissleder and L. Josephson, Nanoparticle– target interactions parallel antibody– protein interactions, *Anal. Chem.*, 2009, **81**, 3618–3622.

199 J. M. Perez, F. J. Simeone, Y. Saeki, L. Josephson and R. Weissleder, Viral-induced self-assembly of magnetic nanoparticles allows the detection of viral particles in biological media, *J. Am. Chem. Soc.*, 2003, **125**, 10192–10193.

200 Y. P. Chen, Y. L. Xianyu, Y. Wang, X. Q. Zhang, R. T. Cha, J. S. Sun and X. Y. Jiang, One-Step Detection of Pathogens and Viruses: Combining Magnetic Relaxation Switching and Magnetic Separation, *ACS Nano*, 2015, **9**, 3184–3191.

201 C. J. Heneghan, E. A. Spencer, J. Brassey, A. Plüddemann, I. J. Onakpoya, D. H. Evans, J. M. Conly and T. Jefferson, SARS-CoV-2 and the role of airborne transmission: a systematic review, *F1000Research*, 2021, **10**, 232.

202 T. Yang and T. V. Duncan, Challenges and potential solutions for nanosensors intended for use with foods, *Nat. Nanotechnol.*, 2021, **16**, 251–265.

203 G. La Rosa, P. Mancini, G. B. Ferraro, C. Veneri, M. Iaconelli, L. Bonadonna, L. Lucentini and E. Suffredini, SARS-CoV-2 has been circulating in northern Italy since December 2019: Evidence from environmental monitoring, *Sci. Total Environ.*, 2021, **750**, 141711.

204 I. D. Amoah, N. P. Mthethwa, L. Pillay, N. Deepnarain, K. Pillay, O. O. Awolusi, S. Kumari and F. Bux, RT-LAMP: a cheaper, simpler and faster alternative for the detection of SARS-CoV-2 in wastewater, *Food Environ. Virol.*, 2021, **13**, 447–456.

205 G. Sriram, M. P. Bhat, P. Patil, U. T. Uthappa, H.-Y. Jung, T. Altalhi, T. Kumeria, T. M. Aminabhavi, R. K. Pai and M. D. Kurkuri, based microfluidic analytical devices for colorimetric detection of toxic ions: A review, *TrAC, Trends Anal. Chem.*, 2017, **93**, 212–227.

206 A. L. Ferreira, L. F. de Lima, M. D. T. Torres, W. R. de Araujo and C. de la Fuente-Nunez, Low-cost optodiagnostic for minute-time scale detection of SARS-CoV-2, *ACS Nano*, 2021, **15**, 17453–17462.

207 K. Wu, R. Saha, D. Su, V. D. Krishna, J. Liu, M. C.-J. Cheeran and J.-P. Wang, Magnetic-nanosensor-based virus and pathogen detection strategies before and during COVID-19, *ACS Appl. Nano Mater.*, 2020, **3**, 9560–9580.